

Approved for public release; distribution is unlimited.

A Method to Determine Small-Scale Internal Wave and Spice Fields from a Single CTD Profile with Application to Three Long-Range Ocean Acoustics Experiments

by F.S. Henyey, J.A. Mercer, R.K. Andrew, and A.W. White

Technical Memorandum
APL-UW TM 1-14
March 2014



Applied Physics Laboratory University of Washington
1013 NE 40th Street Seattle, Washington 98105-6698

Grants N00014-08-1-0843, N00014-07-1-0743, N00014-03-1-0181,
N00014-06-1-0194, and N00014-13-1-0009

ACKNOWLEDGMENTS

The CTD profiles were collected on cruises sponsored by the Long Range/Deep Water Propagation area of the Ocean Acoustics Program at the Office of Naval Research (ONR) under APL-UW grants N00014-03-1-0181, N00014-07-1-0743, and N00014-08-1-0843 and Scripps Institution of Oceanography grant N00014-08-1-0840. This work was also supported by ONR grants N00014-06-1-0194 and N00014-13-1-0009. Dr. A. Ganse and Ms. L. Buck at APL-UW assisted with data processing.

ABSTRACT

The smaller vertical scales of sound speed variability of several recent deep water Pacific Ocean acoustic experiments are extracted from individual conductivity, temperature, depth (CTD) casts taken along the acoustic paths of these experiments, close to the times of the experiments. The sound speed variability is split into internal wave variability and spice variability, as these two parts obey very different dynamics – the internal waves move through the water and the spice field moves with the water. Larger scales are mostly responsible for acoustic travel time fluctuations, but smaller scales are mostly responsible for other important phenomena such as intensity and arrival angle fluctuations. A method is presented to determine when the two components are separable. The internal wave properties are consistent with a spectral model such as a generalized Garrett–Munk model, whereas the spice is very intermittent, and the measurements are not extensive enough to confidently make a spice model for acoustic propagation purposes. Both the internal wave results and the spice results are summarized as vertical wavenumber spectra over a selected vertical depth interval, but with the spice, it must be understood that a spectral model would be very different from the data, and that the three-dimensional horizontal–vertical spectrum would be pure conjecture. The spectral level of the (small-scale) spice, averaged over all the profiles, is comparable to that of the internal waves, suggesting that it is not significantly less important to acoustic propagation than are the (small-scale) internal waves.

This page is blank intentionally.

1 Introduction

In several recent low-frequency, long-range acoustic propagation experiments, a number of deep conductivity, temperature, depth (CTD) profiles were taken to characterize the propagation environment. The characterization of the environment in acoustics experiments is, of necessity, incomplete; the acoustics is the primary concern. In particular, deep CTD profiles are time intensive, and multiple deep profiles at one location are rarely taken. Thus, the time dependence of the measured profile is not known directly. Time dependence, when available, is used to extract sound speed fluctuations from a background sound speed profile. Here, a method is developed to estimate the smaller scale fluctuations from single profiles. Moored CTD instruments provide a complementary view of fluctuations. For these measurements, time series are obtained, but the vertical resolution is necessarily much coarser than with a CTD profile. For example, in one of the experiments considered here moorings deployed had inter-sensor spacings of 30–140 m over our depth range of interest; fluctuations with wavelengths twice those scales and larger were extracted from the sensor data [3]. In contrast, our largest scale is on the order of 100 m in the vertical.

Experimental data considered here are from the Long-Range Acoustic Propagation Experiment (LOAPEX [12]), 10 September – 10 October 2004; the Philippine Sea pilot study (PhilSea09), 14 April – 1 May 2009; and the Philippine Sea Experiment (PhilSea10) [16], 5–29 May 2010. Here, we analyze acoustically relevant fluctuations in the profiled CTD measurements made during these experiments. Both internal waves and spice are of interest. The internal waves and spice are put on a comparable quantitative scale in terms of their influences on the sound speed. Specifically, we calculate a vertical displacement of density from an equilibrium background density stratification and a vertical displacement of sound speed from a background sound speed profile.

LOAPEX includes seven CTD profiles taken at acoustic source stations along a 3200-km path from a receiver mooring. In addition, there was a profile taken north of the island of Kauai. PhilSea09 includes 19 CTD profiles taken during three cruises between acoustics moorings. PhilSea10 includes 51 CTD profiles taken every 10 km along a 500-km path from a receiver mooring. Every fifth PhilSea10 profile samples the entire water column, while the other four extended to about 1500 m depth. The receiver moorings in PhilSea09 and PhilSea10 were in the same place, and were the southwest end of the PhilSea09 CTD line and the northwest end of the PhilSea10 CTD line. This report presents results in the form of spectra for a few of the profiles, and several average spectra. The complete set of available spectra is presented in the Appendix.

The primary goal of our method is to extract the small-scale internal wave and spice fields from a single profile. The small scales are defined here to have vertical wavelengths smaller than about 100 m. Larger scale features, in a single CTD profile, cannot be distinguished from structure in the background. The larger scales are mostly responsible for acoustic travel time fluctuations, but the smaller scales are mostly responsible for other phenomena such as the intensity and arrival angle fluctuations. The assumption is made that the

smaller scales in density and sound speed are the internal waves and spice of interest. This assumption is tested at every place and time, as described below. It is possible that the background stratification at some places and times has smaller structures, requiring the test to be done everywhere.

The method described here is based on the familiar approximate relation that the density ρ differs from a reference background density profile ρ_0 by the density displacement ζ_ρ times the non-adiabatic density gradient

$$\rho - \rho_0 = \zeta_\rho \left(\frac{\partial \rho_0}{\partial z} \right)_{\text{na}} \quad (1)$$

and a corresponding relation based on sound speed

$$c - c_0 = \zeta_c \left(\frac{\partial c_0}{\partial z} \right)_{\text{na}} . \quad (2)$$

Formal measurements of the ‘reference’ quantities cannot be determined from single CTD casts, and therefore the following approximations are made. Given only a single cast, the background sound speed (treatment for the density is identical) is approximated by the low-pass filtered sound speed, and the non-adiabatic background sound speed gradient is approximated with the vertical derivative of the low-pass filtered sound speed. Because the low-pass filtering cannot distinguish between the background structure and the low-mode perturbations, the approximate ζ_c represents, at best, the high-mode components of the perturbation field. However, as mentioned previously, the quantities of interest here are the smaller scales of the internal wave and spice fields. Unfortunately, the approximation for the reference sound speed gradient does not work well in all cases, as the non-adiabatic gradient can be small or even negative. The method presented here cannot be used for profiles in which that is the case.

2 Processing

The initial stages of the processing were done with Seabird software [15]. This processing converted the raw data to conductivity, temperature, and pressure, adjusted the measurement time constants, and calculated the practical salinity. (Unfortunately, some salinity spiking remained, which can overwhelm legitimate small-scale fluctuations at high wavenumbers.) The outputs used from the Seabird software were pressure, temperature, and salinity. The next step of the processing uses the thermodynamic equation of state for seawater [8]. This equation of state has two very important properties:

1. It is consistent thermodynamically. The fundamental expression is for the Gibbs free energy G as a function of pressure, temperature, and practical salinity. All other state quantities are calculated in terms of derivatives of this function. (See, for example,

Müller [13].) Automatically, the adiabatic lapse rate of density is the reciprocal of the square of the sound speed. (Here, the adiabatic lapse rate of any quantity Q means the adiabatic derivative of Q with respect to pressure, which we write as $(\partial Q/\partial P)_{\text{ad}}$.)

2. The formula for G was based on a least squares fit of various data, and that data included the Del Grosso sound speed [6], which is thought to be the most accurate sound speed formula in the deep ocean [7]. This makes all quantities more accurate in the deep ocean.

Various derivatives of the Gibbs function representation [8] up to third order were calculated. (Some third order derivatives are needed for the adiabatic lapse rate of sound speed.) The depth was calculated by integrating the hydrostatic equation. The results are interpolated onto a uniform depth grid. The outputs of this step are depth, pressure, density, sound speed, and the adiabatic lapse rates of density and sound speed. A consistent depth interval of 50 m to 1480 m was selected for all profiles. This depth interval is, or contains, the depths of most acoustical interest, which are the regions of the acoustic upper turning points. The choice of 50 m for the top was made to avoid the observed surface mixed layer. Many of the profiles did not go below 1480 m, determining our lowest depth.

Next, sloping straight line trends are removed from the density and sound speed profiles, leaving detrended curves that vanish at the end points. Further processing is performed in the vertical wavenumber Fourier domain. The density and sound speed are not stationary Gaussian processes, so the common practice of using windowed exponential Fourier transforms would weight different parts of the depth range unequally. Instead, we use sine and cosine transforms as described below, which weight different regions more equally. Of the various types of such transforms, type I transforms [10] are appropriate when data are specified on equally spaced points that include the top and bottom points. The detrended curves are sine transformed: the trend line will be associated later with the value at vertical wavenumber $k_z = 0$.

The next step is to split the density and sound speed data into a low-pass part and a high-pass part. To prevent ringing, a taper in wavenumber space was applied. The taper is $\cos^2(\pi k_z/4k_c)$, $0 \leq k_z \leq 2k_c$ where $k_c = 2\pi/100$ m is the half-amplitude cutoff wavenumber. The derivative of the low-pass component is calculated by multiplying the tapered sine transform by k_z , and inverse cosine transforming after including the slope of the separated straight line as the $k_z = 0$ part. The adiabatic derivative of density is the adiabatic lapse rate times the numerically calculated derivative of the pressure with respect to depth. The non-adiabatic derivative of the low-pass part is the difference between the derivative of the low-pass part and the adiabatic derivative of the low-pass part. The buoyancy frequency squared ([13], Eq. 6.83) is the non-adiabatic derivative of the low-pass filtered density multiplied by $-g/\rho$, or equivalently,

$$N^2 = g^2 \left(\frac{d\rho}{dP} - \left(\frac{\partial \rho}{\partial P} \right)_{\text{ad}} \right). \quad (3)$$

The high-pass part is defined as the inverse sine transform of the total minus the low-pass part. We postulate that the high-pass part contains primarily the fluctuations due to internal waves and spice, while the derivative of the low-pass part is dominated by the derivative of the background (and the large-scale fluctuations, which cannot be separated from the background.)

Following (1) and (2) the density and sound speed displacements are calculated by dividing each high-pass component by the non-adiabatic derivative of the corresponding low-pass component. The Garrett–Munk (GM) model predicts the high-pass internal wave spectrum to be stationary. However, we do not want to assume this model result in our analysis, and moreover we do not have any expectation for the spice displacements, so a sine transform is appropriate. By construction, the displacements vanish at the top and bottom. The sine transforms are calculated and squared to yield periodograms of the displacements (hereinafter spectra), and multiplied together to yield cross-periodograms (hereinafter cross-spectra) between the density and sound speed displacements. These periodograms are pre-whitened by multiplying by k_z^2 ; this essentially yields strain periodograms. The spectral estimates are obtained by smoothing the strain periodograms. Each sine periodogram value, considered as a spectral estimate, has a variance equal to twice the square of the spectral value. The particular smearing used reduces the variance of the spectral estimates by more than a factor of 20 from that of the periodogram. If the displacements and strains are not stationary processes, the spectra must be understood as power spectra averaged over the depth range.

The displacement spectra are rapidly decreasing, so one gets a much smaller dynamic range with the strain spectra (i.e., by pre-whitening), allowing plots that show much more detail. The less variable spectrum decreases the severity of aliasing and distortion of the spectrum due to the smearing. The second reason only applies to the internal waves. The GM spectrum, which makes a Wentzel–Kramers–Brillouin (WKB) approximation, gives a very simple description of the strain spectrum: the vertical wavenumber spectrum, except for the first few modes, is constant in wavenumber and depth.

For the “GM79” version [5] of the GM spectrum, the strain spectrum has the value 0.275 m for wavenumbers in rad/m, or 1.73 for wavenumbers in cpm. Munk describes a saturation cutoff, empirically at a 10-m wavelength, where the shear rate variance divided by N^2 is “of order 1.” Beyond that cutoff, the shear or strain spectrum falls proportional to $1/k_z$. The strain variance in the GM79 model is one-third the variance of the ratio of shear to buoyancy frequency. As a result, the strain spectral level times the cutoff is 0.173, given the Munk values. Beyond the cutoff, the strain spectrum is $0.173/k_z$ (where k_z is in cpm).

Fig. 1 shows the effects of the high-pass filter and the spectral smoothing on the GM79 spectrum. Results from the data must be interpreted with the high-pass filter in mind. The sound speed displacement can be thought of as made up of the sum of two parts, the spice and density displacements. If the water parcel were moved adiabatically to a depth at which its density is the reference density, it would be moved by the negative of its density

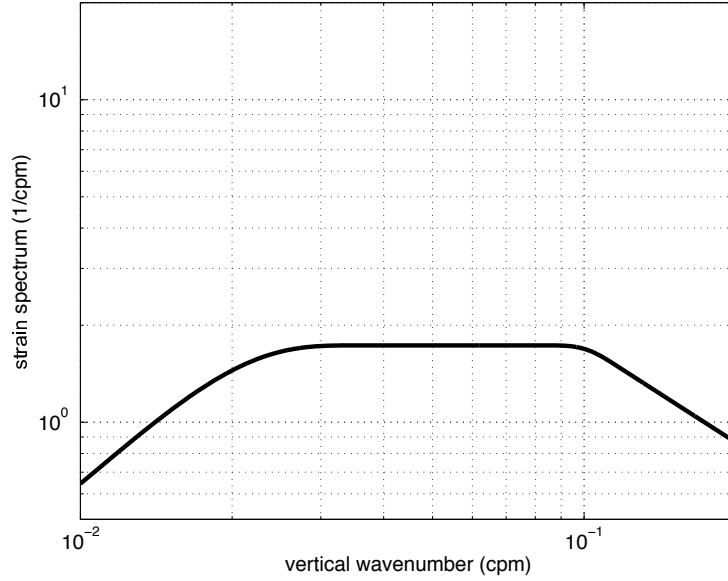


Figure 1: The effect of our processing method on the Garrett–Munk internal wave strain spectrum. The normalization is the GM79 version [5]. The low wavenumbers are suppressed by the high-pass filter, and the suppression is spread to somewhat higher wavenumbers by the smoothing of the spectrum. The Munk cutoff at high wavenumbers is included.

displacement. However, it still might not have the reference sound speed. It would have to be moved adiabatically an additional negative of the spice displacement to make its sound speed equal to the reference sound speed. Internal waves move through the water, while spice fluctuations move with the water. The phase of the waves changes linearly with time relative to the spice, so one expects no correlation between the density displacement and the spice displacement. This pair of assumptions, that the density fluctuations are internal waves and that these waves are uncorrelated with spice, can be tested. The displacements are

$$\begin{aligned}\zeta_\rho &= \zeta_{IW} \\ \zeta_c &= \zeta_{IW} + \zeta_{spice}.\end{aligned}$$

Under the assumptions made above, the correlation functions are

$$\begin{aligned}\langle \zeta_\rho(z_1)\zeta_\rho(z_2) \rangle &= \langle \zeta_{IW}(z_1)\zeta_{IW}(z_2) \rangle \\ \langle \zeta_\rho(z_1)\zeta_c(z_2) \rangle &= \langle \zeta_{IW}(z_1)\zeta_{IW}(z_2) \rangle + \langle \zeta_{IW}(z_1)\zeta_{spice}(z_2) \rangle \\ &= \langle \zeta_{IW}(z_1)\zeta_{IW}(z_2) \rangle \\ \langle \zeta_c(z_1)\zeta_c(z_2) \rangle &= \langle \zeta_{IW}(z_1)\zeta_{IW}(z_2) \rangle + \langle \zeta_{IW}(z_1)\zeta_{spice}(z_2) \rangle \\ &\quad + \langle \zeta_{spice}(z_1)\zeta_{IW}(z_2) \rangle + \langle \zeta_{spice}(z_1)\zeta_{spice}(z_2) \rangle \\ &= \langle \zeta_{IW}(z_1)\zeta_{IW}(z_2) \rangle + \langle \zeta_{spice}(z_1)\zeta_{spice}(z_2) \rangle.\end{aligned}$$

These relations can be Fourier transformed into spectra. The density displacement spectrum and the density–sound speed cross spectrum are predicted to be equal, both equal to the internal wave displacement spectrum. The imaginary part of the cross spectrum should be zero. The sound speed displacement spectrum is larger, and is equal to the sum of the density displacement and spice displacement spectra. This is the fundamental test. In some cases, these tests would fail. For example, in the C-SALT area [14] off the northeast coast of South America, a double-diffusive process mixes the water in steps sufficiently rapidly to overcome the dynamical effect of internal wave propagation. Thus, on the scale of the steps, the density displacement and spice displacement are correlated.

Submesoscale vortices [11] typically have a spice signature as well as a small vertical density displacement relative to the surrounding water, so they would also yield a small correlation. Larger vortical-mode features, such as mesoscale eddies, also have both spice and density variability, but we consider these much larger features to be part of the background; in any case, they are eliminated by the high-pass filter. These examples show that the tests of the assumptions should be made in every case.

In addition, the tests may be successful, but the results would still not be valid. Spice fronts temporarily reversing the general trend of the sound speed profile can violate the use of low-pass derivatives to estimate sound speed displacements. Several profiles from the experimental data considered here had such fronts (Fig. 2), but were eliminated from analysis so as to have consistent processing for the remainder. The density profile, when low-pass filtered, has a nearly constant derivative in the depth interval shown, so density displacements are estimated accurately, but if the sound speed is low-passed, the derivative is very small, and is sensitive to the parameters of the low-pass filter, so the corresponding displacements are very large and meaningless.

These fronts are clearly relevant to acoustic propagation, but in a way different from the oscillating fluctuations that our method can handle.

3 Examples

3.1 LOAPEX

Eight CTD profiles were taken at locations where the acoustic projector was deployed to transmit to a pair of vertical line arrays (VLA) of receivers. The first seven locations were along a great circle. The location of the VLA was $33.4^{\circ}\text{N } 222.3^{\circ}\text{E}$ and the farthest station was at $34.6^{\circ}\text{N } 187.5^{\circ}\text{E}$. These transmission stations are identified by their distance in kilometers from the VLA as T50, T250, T500, T1000, T1600, T2300, and T3200. The last profile was taken a short distance north of the island of Kauai.

Each of the first four profiles had spice fronts leading to unrealistic ‘sound speed displacements’. Therefore, these profiles are excluded from this study, even though a modified

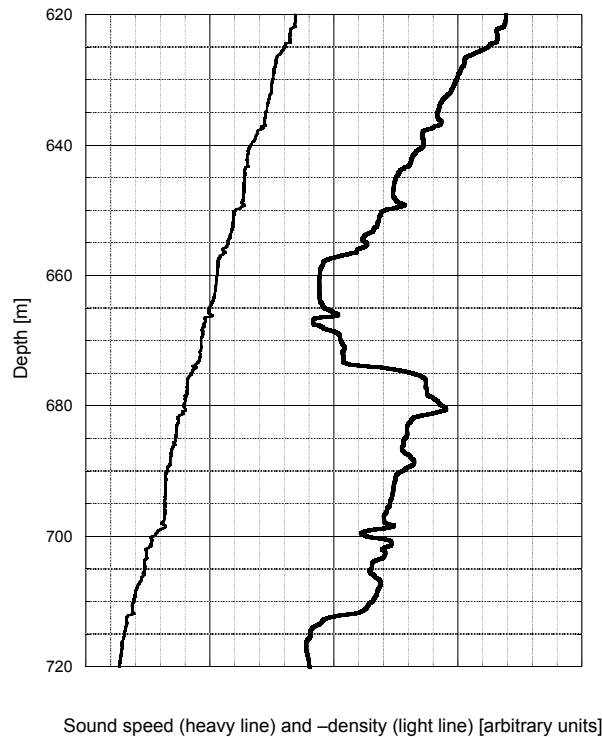


Figure 2: A 100-m section of a CTD profile, showing a spice front that invalidates the derivative formula for sound speed displacement. The density profile shows no features at this front, so the density displacement is given correctly by the corresponding formula. Profiles such as this are excluded from the analysis presented here.

algorithm could yield meaningful results.

The T1600 profile was taken at a station located at 35.3°N , 154.9°W . It is about several hundred kilometers away from either of the two major North Pacific fronts, the subpolar and subtropical fronts. Thus, it might be expected to have less spice than locations close to one of these fronts.

An upper section (400–500 m) from the vertical profiles of the density and sound speed displacements at station T1600 shows that the two are approximately the same (Fig. 3a); little spice is evident. A lower section (900–1000 m) shows that the two displacements differ (Fig. 3b). Although the (high-pass) density displacements resemble a stationary Gaussian process, the spice is very intermittent, being present in one of these sections, but almost non-existent in the other. This spatial intermittency occurs throughout all profiles. Plots of strain spectra (Fig. 4) show density and cross-spectra as approximately equal, completing the test successfully, and the sound speed spectrum is consistently larger than the others.

The density spectrum rises initially, due to the high-pass filter of the processing, looking similar to the reference GM79 curve (Fig. 1). Beyond the rise, it is roughly constant. The

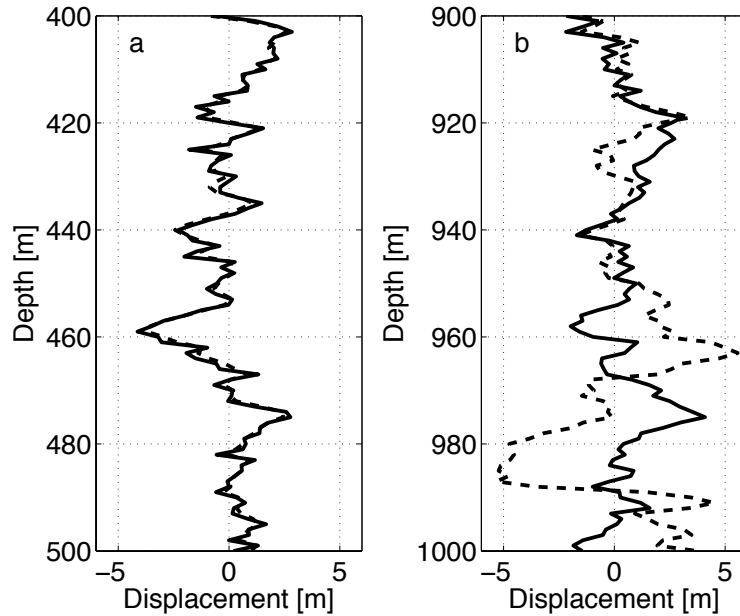


Figure 3: Sections of the LOAPEX T1600 displacement profiles, showing spice intermittency. The density displacement is the solid curve and the sound speed displacement is the dashed curve. From 400 m to 500 m (a), the two curves are almost identical, showing almost no spice fluctuations. From 900 m to 1000 m (b), the curves are very different, showing the presence of significant spice fluctuations.

level in the rise and beyond is about half the strength of the GM model, which has been found to apply generally to the Northwest Pacific [2, 4]. Munk's arguments imply that the break for a half-strength spectrum should be at twice the wavenumber shown in the comparison curve, or about 0.2 cpm. This delayed break is consistent with the data. No spectra are shown beyond 0.2 cpm, as salinity spiking becomes important at about that value. The sound speed strain spectrum is about 50% larger than the density displacement spectrum at smaller wavenumbers, rising to about twice the density displacement spectrum at larger wavenumbers. If we take the spectral levels as an indication of the importance to acoustics, the spice is about half as important to equally important as the internal waves averaged over this profile. However, as can be seen by comparing the two displacements (not shown), there is very little spice between 200 m and 900 m. The minimum sound speed is around 750 m deep, so any acoustic propagation with an upper turning point below 200 m is affected very little by spice at this location.

T2300 and T3200 are on about the same latitude as T1600, and the spectra are similar to those of T1600, but for these profiles, there is significant spice in the 200–900-m region. The average of the three spectra are shown in Fig. 5. All four strain spectra results are provided in Appendix 1.1. The density strain spectral level is about half of GM79, and the spice strain is slightly larger than the density strain. The Kauai station is in a different oceanographic region than the stations described previously. The internal wave spectral

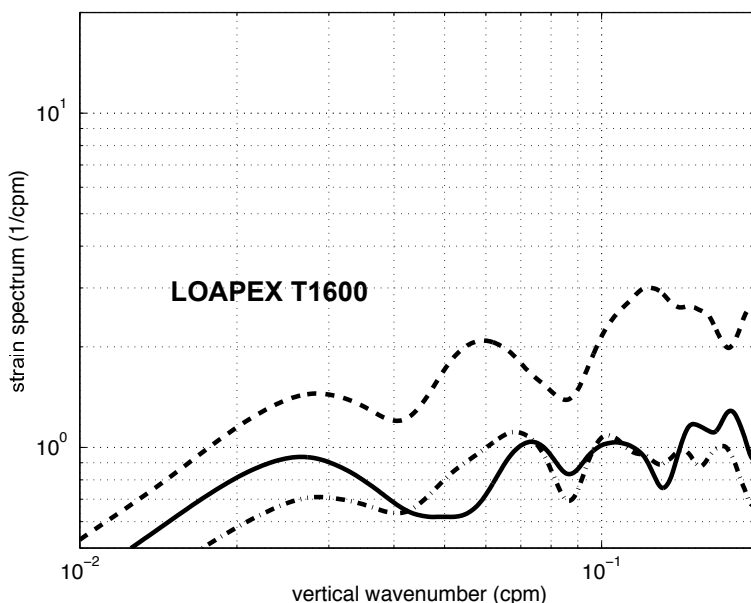


Figure 4: The spectra from LOAPEX T1600. The solid curve is the density strain spectrum, the dashed curve is the sound speed strain spectrum, and the dot-dash curve is the cross spectrum. From the assumption of the lack of correlation between internal waves and spice, the density strain spectrum and the cross spectrum should both equal the internal wave spectrum, and therefore be equal, which is approximately true. Their level is about half the GM79 level (Fig. 1). The spice spectrum is the difference between that of the sound speed and that of the density. The level of the spice spectrum is close to that of the internal wave spectrum for this profile.

level is larger, more than twice the GM79 value (Fig. 6). There appears to be a break in the spectrum at about the wavenumber 0.04 cpm, in agreement with Munk's prediction.

3.2 PhilSea09

The main acoustic VLA mooring was located near 21.4°N, 126°E. The CTD profiles taken during PhilSea09 extended in a NNE direction to near 22.96°N, 126.56°E, a distance of 182 km at a compass heading of 18°.

Nineteen CTD casts made during the 2009 Philippine Sea Pilot Study/ Engineering Test [16] are analyzed. These casts were made from the R/V *Melville* during three instrument deployment and recovery cruises. (See Fig. 7.) These casts spanned the period 2 April – 12 May 2009, and sampled a 183-km section.

Several types of spectra were calculated from the CTD data. Spectra indicating very little spice are evident (Fig. 8). Other spectra had stronger contributions, e.g., cast G

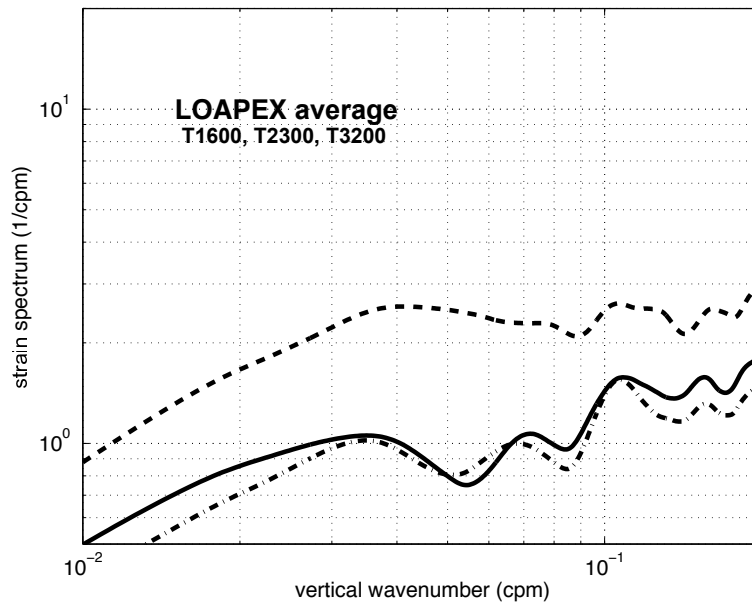


Figure 5: The average of the three spectra from LOAPEX stations near 35° latitude without spice fronts. The curves in this and other figures represent the same spectra as in Fig. 4. The cross spectrum is closer to the density strain spectrum than it was for a single station. The internal wave level is about half GM79. The spice spectrum (the difference between the dashed and solid curves) is larger than the internal wave spectrum.

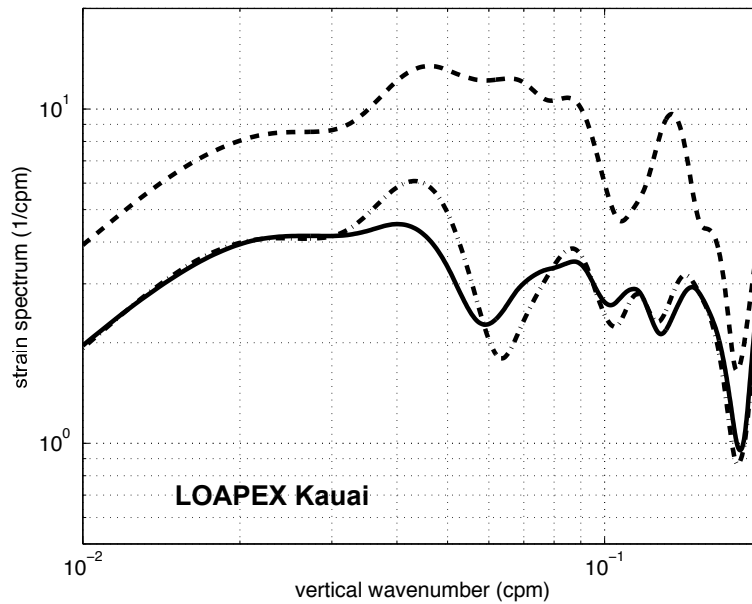


Figure 6: The spectra from the Kauai station. The internal wave level is more than twice the GM79 level, and there is an apparent spectral slope change at about 0.04 cpm, consistent with Munk's argument.

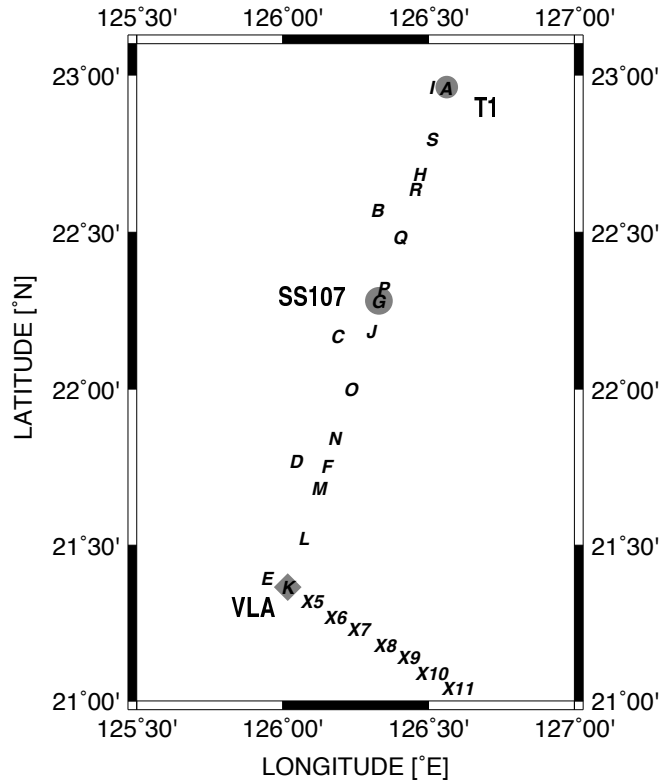


Figure 7: The positions of the PhilSea 09 CTD stations, labeled A through S, and a few of the PhilSea 10 stations labeled X5 through X11 (X4 and K were in almost the same place).

(Fig. 9). For this cast, the spice contribution is almost as strong as the internal wave contribution. Little is known about the spatial structure of spice, other than that it is ‘intermittent’. Casts made near the VLA measured consistently low levels of spice intensity. Casts made further north generally measured higher levels of spice. Colosi and coworkers [3] suggest that spice contributions to sound speed anomalies were small at the VLA, in agreement with our analysis (Fig. 8). Relative density and sound speed anomaly maps made from all the CTD profiles along the section (Fig. 10) do not in general show a clear pattern of fronts, eddies, or intrusions that might suggest the presence of spice. This is expected because the cast programs on the three cruises were not organized into a regular space–time sampling program, and further, the casts span more than one month.

The average spectra for the entire set, excluding several that had distinct identifiable fronts, is shown in Fig. 11. All the strain spectra are provided in Appendix 1.2. The cross spectrum is almost exactly the same as the density spectrum (except for the small salinity spiking effect), showing that the assumptions of our processing are valid. Though spice level is less than the internal wave level, it is substantial.

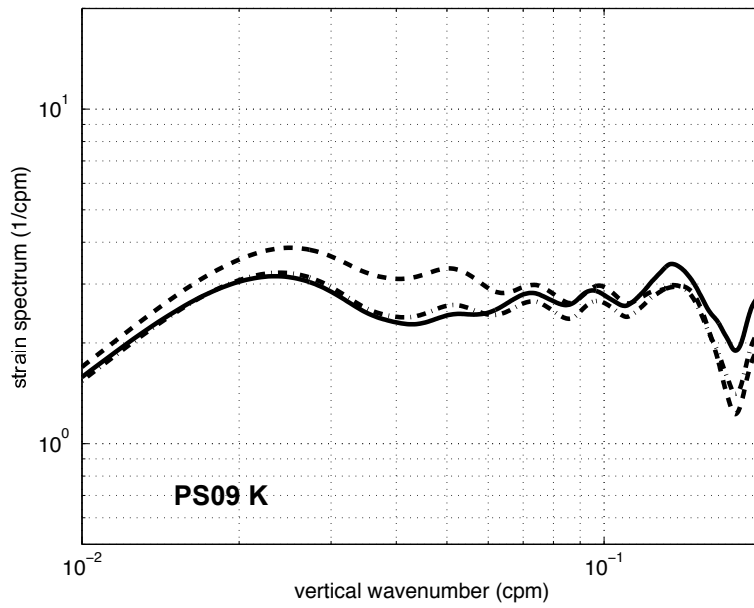


Figure 8: The spectra for a profile measured at the receiver mooring, PhilSea09. This profile has a small amount of spice fluctuations. The internal wave level is somewhat higher than GM79.

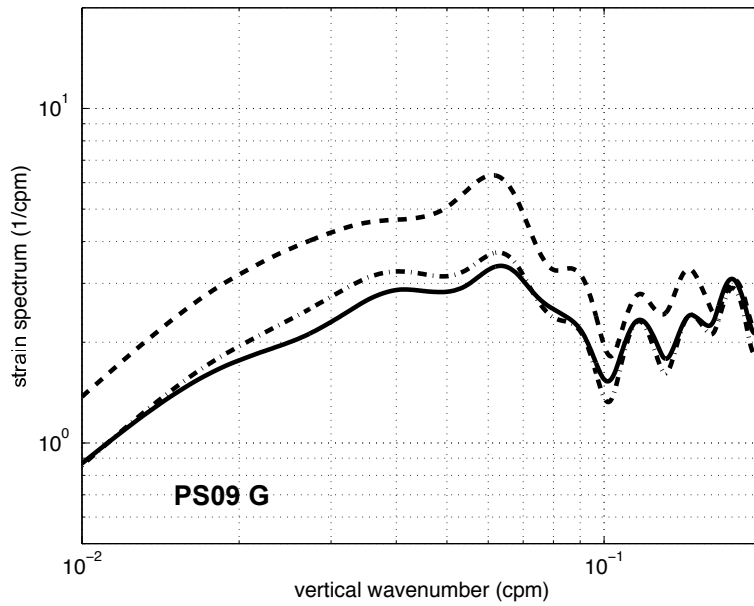


Figure 9: Spectra from PhilSea09 profile G. This profile has more spice, and its shape is somewhat different than the GM79 spectrum.

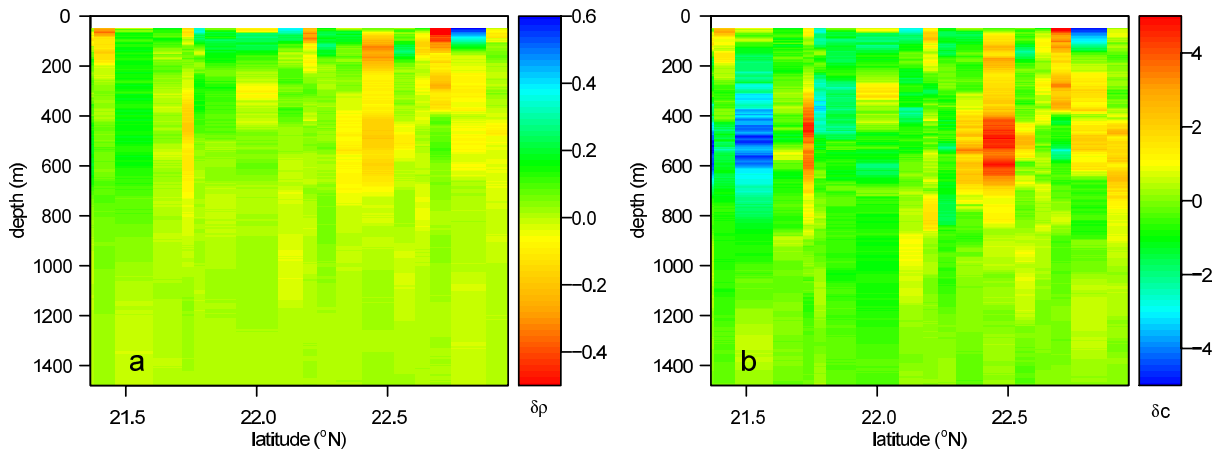


Figure 10: The large-scale density (a) and sound speed (b) anomaly fields in the PhilSea09 transect. The anomaly is defined as the difference between the measured values and the horizontal average at each depth. No clear pattern is evident, although the northern half of the observations suggests a more complex assembly of warm water parcels.

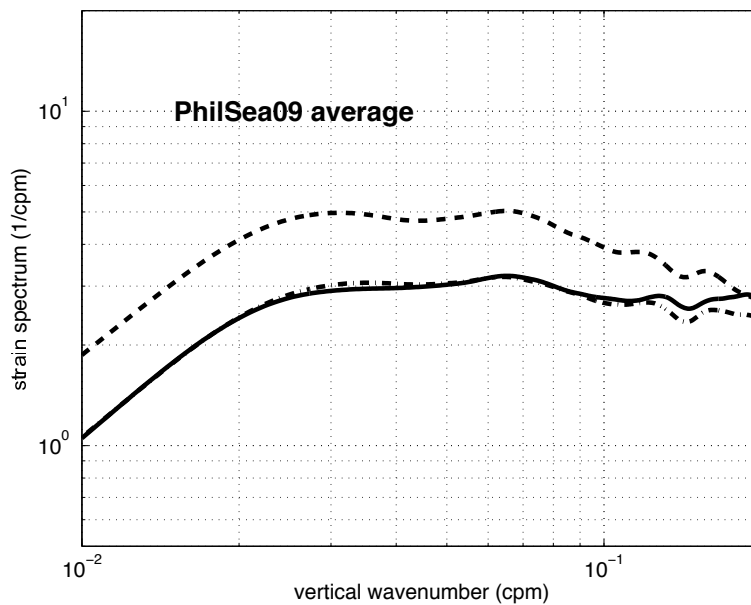


Figure 11: The average spectra from PhilSea09 profiles without spice fronts. The internal wave level is 1.7 times GM79, and the spice is 1.2 GM79.

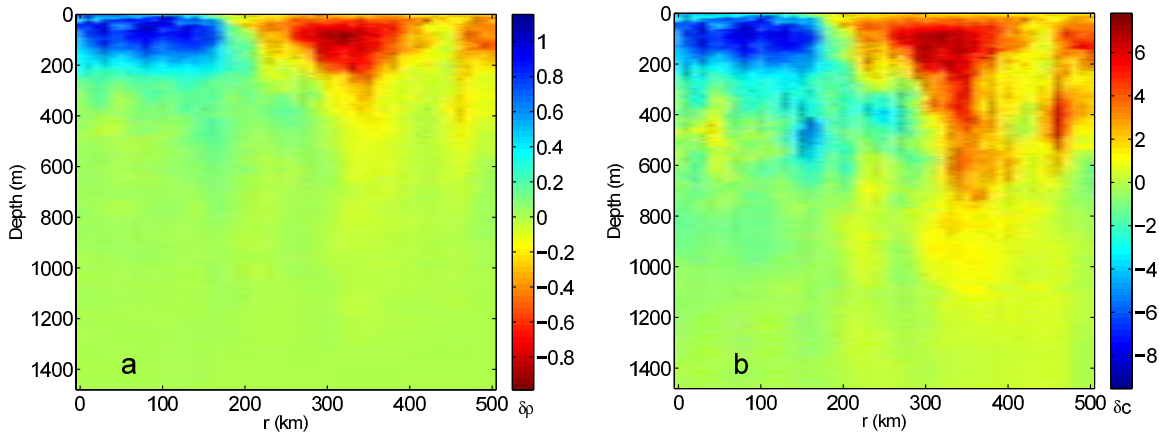


Figure 12: The large-scale density (a) and sound speed (b) anomaly fields in the PhilSea10 transect. The anomaly is defined as the difference between the measured values and the horizontal average at each depth. The western side is a relatively constant colder region, and there is a rather wide transition to a warmer and less constant region in the center and eastern part of the transect. The transition was verified to be in geostrophic balance using the measured current. The sound speed structure extends deeper than the density structure.

3.3 Philsea10

Fifty-one CTD profiles were taken every 10 km along a 500-km path at a compass heading of 121° , starting near the acoustic VLA mooring. Thus, the PhilSea09 and Philsea10 CTD lines almost coincided at their start points, and went in directions about 103° apart. There were several other profiles taken, which we do not discuss; the 500-km path consists of profiles numbered from #4 at range 0 to #54 at range 500 km.

The large-scale variability of sound speed and density along this path are characterized by a relatively uniform region for the first 170 km, with a much more variable contrasting region beyond that point (Fig. 12). The sound speed variability extends considerably deeper than the density variability. From the comparison with the ship's acoustic Doppler current profiler (ADCP) data and the density variation between these two regions, it was verified that the two regions are in geostrophic balance, as expected.

In the first 110 km (twelve profiles, #4 through #15), well within the relatively uniform region, very little spice fluctuation was observed. Profile #12 is the most spice-free of all (Fig. 13); the three spectra are almost identical. A small effect of salinity spiking is apparent on the density strain spectrum at the highest wavenumbers; it becomes larger at the wavenumbers beyond those plotted. The average of profiles taken in the first 110 km is shown in Fig 14. The density strain spectral level is about 75% larger than GM79. It is interesting that this region of little spice abuts the region of little spice observed one year earlier during PhilSea09.

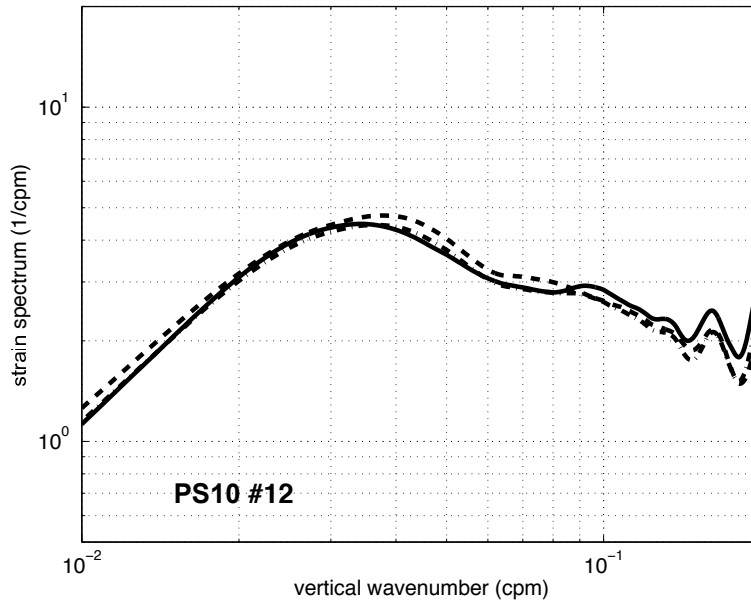


Figure 13: The PhilSea10 spectra from profile #12 with the smallest spice fluctuations.

Farther southeast, the amount of spice strain increases and the amount of density strain decreases. An example is profile #38 (Fig. 15). The average of the remainder of the profiles has a spectral level about 25% larger than GM79. The average for the entire set is shown in Fig. 16 and the entire set of strain spectra results is presented in Appendix 1.3. With this average of a large number of profiles, the cross spectrum is almost exactly the same as the density spectrum (except for the small salinity spiking effect), showing that the assumptions of our processing are valid. Though the spice level is less than the internal wave level, it is substantial.

Fig. 17 shows the spice field spatial characteristics along the PhilSea10 transect, plotting for each cast the difference between the strain spectrum calculated with the sound speed and the strain spectrum calculated with the density. Regions with little spice have a difference near zero. The bright red/orange regions indicate profiles (hence ranges) where there was considerable spice detected in the profile. This transect shows that spicy regions may be compact and localized.

4 Discussion

The processing to extract internal waves and spice from single CTD profiles satisfies validity tests, giving credibility to the spectra that have been calculated. The density strain spectrum measures the high-wavenumber internal wave strength, and the sound speed strain spectrum measures the sum of the internal wave and spice strengths.

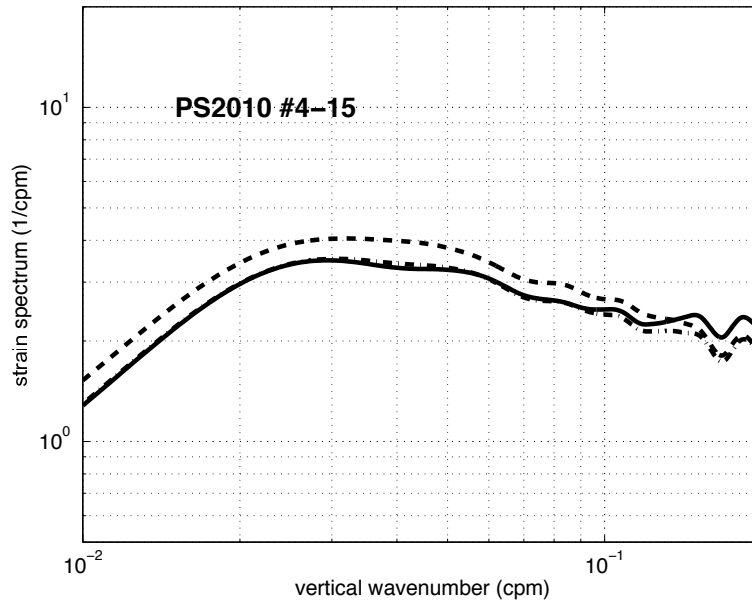


Figure 14: The average spectra of the first 12 profiles from the westernmost 110 km of the PhilSea10 transect. There is very little spice, and the internal wave spectral level is nearly twice the GM79 level. This region lies within the nearly constant colder region of the large-scale density and sound speed structure. Its west end is at the VLA mooring, where there was also very little spice in PhilSea09, one year earlier.

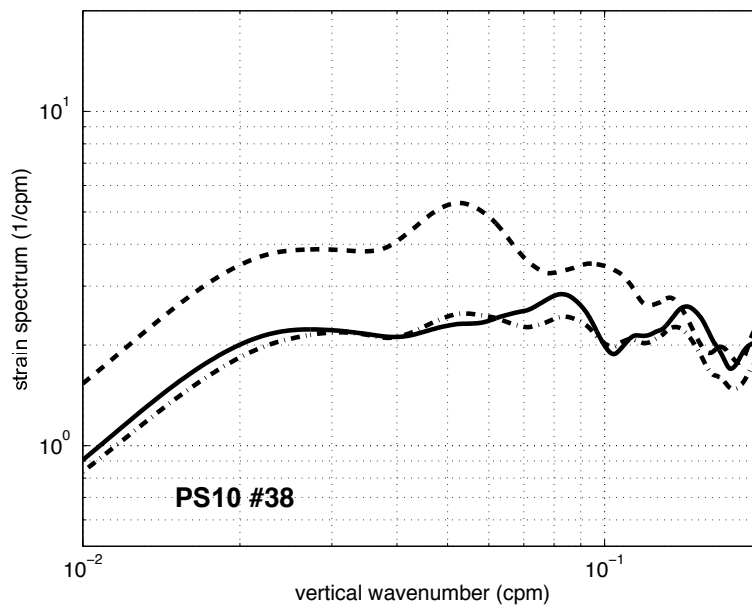


Figure 15: The spectra from profile #38 in the eastern part of the transect. Here the internal waves are only slightly above GM79, and the spice nearly equals the internal waves.

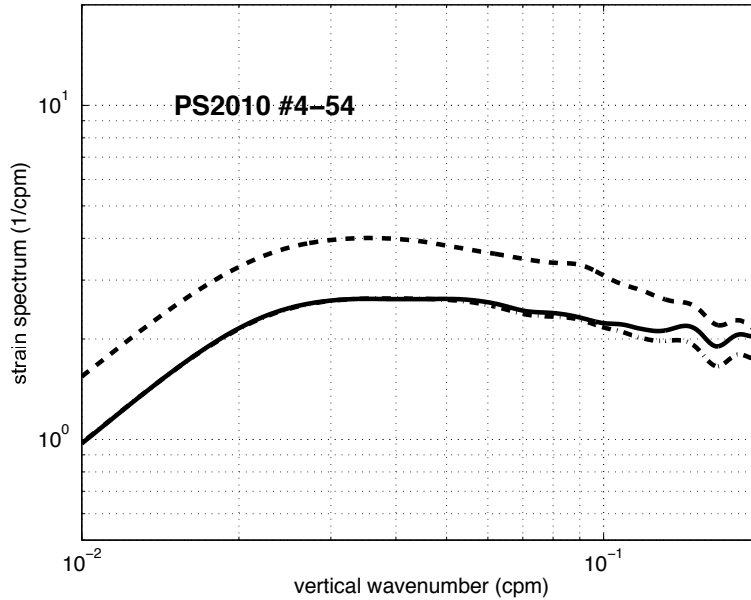


Figure 16: The average spectra from the PhilSea10 transect. The average internal wave level over the entire set is less than that over the first 110 km, but still above GM79. The level of the spice is close to the GM79 reference level.

The internal wave spectra are close to the GM79 shape, and their levels fit the GM assertion that they are mostly within a factor of two of their reference level. In this case, the strain reference level used is GM79, which differs from the reference level of the earlier GM model for the same total internal wave energy [9]. The internal wave level varies with geography, being small along the LOAPEX path and large in the Kauai region and in the Philippine Sea, with even a significant variation along the PS10 path.

The spice level is defined to reflect the importance of its acoustic effects. However, there is a significant uncertainty in such an identification. The spice is not well described by a spectral model. It is highly intermittent, and the response of the acoustics to this intermittency is not known. Moreover, the fluctuations in acoustic propagation depend on the simultaneous horizontal and vertical scales of the sound speed fluctuations, and the analysis presented here determines only the vertical scales. If the aspect ratio of the spice is about the same as the aspect ratio for internal waves, the spectral levels reported here are more likely to be useful in relating the relative importance of the two phenomena. We are far from being able to propose a model for the spice to be used in acoustic propagation calculations, but the levels found here suggest that it is comparable to the effects of internal waves.

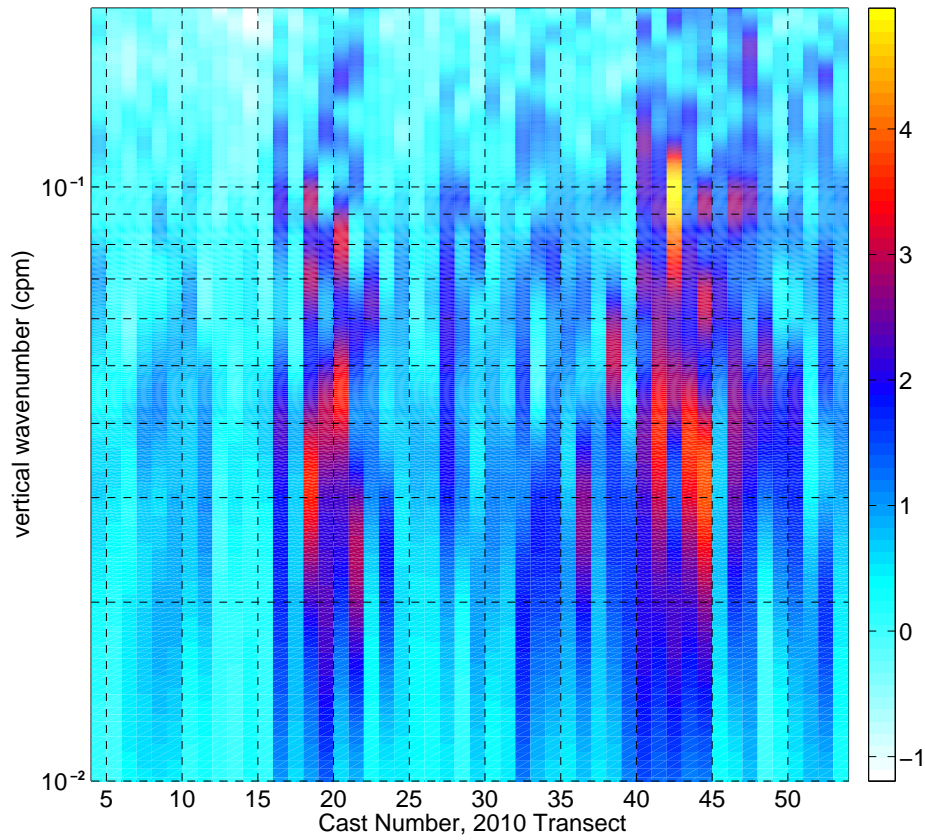


Figure 17: Spatial characteristics of this estimator along the PhilSea2010 transect. The figure shows the difference between the strain spectrum calculated from the sound speed and the strain spectrum calculated from the density. The horizontal axis is cast number: the casts are roughly 10 km apart. The leftmost cast is near the VLA, and the casts trend ESE. The color scale is in units of reciprocal cycles per minute.

References

- [1] J.A. Colosi, 1999. *Data Report for NPAL Internal Wave Environmental Data, IW98 Cruise*, Woods Hole Oceanographic Institution, 54 pp.
- [2] J.A. Colosi, 1997. Random media effects in basin-scale acoustic transmissions, in *Monte Carlo Simulations in Oceanography*, Proceedings of the 9th ‘Aha Huliko’a Hawaiian Winter Workshop, University of Hawaii at Manoa, 14–17 January, P. Müller and D. Henderson, eds., pp. 157–166.
- [3] J.A. Colosi, B.D. Dushaw, R.K. Andrew, L.J. van Uffelen, M.A. Dzieciuch and P.F. Worcester, 2103. Space-time scales of sound-speed perturbations observed in the Philippine Sea: Contributions from internal waves and tides, eddies, and spicy thermohaline structure, *J. Acoust. Soc. Am.*, 134, 3185–3200.
- [4] J.A. Colosi, S.M. Flatté and C. Bracher, 1994. Internal-wave effects on 1000-km oceanic acoustic pulse propagation: Simulation and comparison with experiment, *J. Acoust. Soc. Am.* 96, 452–468.
- [5] W.H. Munk, 1981. A survey of internal waves and small-scale processes, in *Evolution of Physical Oceanography*, B.A. Warren and C. Wunsch, eds., Cambridge, MA: MIT Press.
- [6] V.A. Del Grosso, 1974. New equation for the speed of sound in natural waters (with comparisons to other equations), *J. Acoust. Soc. Am.*, 56, 1084–1090.
- [7] B.D. Dushaw, P.F. Worcester, B.D. Cornuelle and B.M. Howe, 1993. On equations for the speed of sound in seawater, *J. Acoust. Soc. Am.*, 94, 255–275.
- [8] R. Feistel and E. Hagen, 1995. On the GIBBS thermodynamic potential of seawater, *Progr. Oceanogr.*, 36, 249–327.
- [9] A.E. Gargett, 1990. Do we really know how to scale the turbulent kinetic energy dissipation rate ϵ due to the breaking of oceanic internal waves? *J. Geophys. Res.*, 95, 15,971–15,974.
- [10] S.A. Martucci, 1994. Symmetric convolution and the discrete sine and cosine transforms, *IEEE Trans. Sig. Proc.*, 42, 1038–1051.
- [11] J.C. McWilliams, 1985. Submesoscale, coherent vortices in the ocean, *Rev. Geophys.*, 23, 165–182.
- [12] J.A. Mercer, J.A. Colosi, B.M. Howe, M.A. Dzieciuch, R. Stephen and P.F. Worcester, 2009. LOAPEX: The Long-Range Ocean Acoustic Propagation Experiment, *IEEE J. Ocean. Eng.*, 34, 1–11.
- [13] P. Müller, 2006. *The Equations of Oceanic Motions*, Cambridge University Press.

- [14] R.W. Schmitt, H. Perkins, J.D. Boyd and M.C. Stalcup, 1987. C-SALT: An investigation of the thermohaline staircase in the western tropical North Atlantic, *Deep-Sea Res.*, 34, 1697–1704.
- [15] Sea-Bird Electronics, Inc. *Seasoft V2: SBE Data Processing*, Bellevue, WA, <http://www.seabird.com/software/SBEProcforWindows.htm>, last accessed 2012.10.30.
- [16] P.F. Worcester, R.K. Andrew, A.B. Baggeroer, J.A. Colosi, G.D. D’Spain, M.A. Dzieciuch, K.D. Heaney, B.M. Howe, J.N. Kemp and J.A. Mercer, 2013. Acoustic propagation and ambient noise in the Philippine Sea: The 2009 and 2010 – 2011 Philippine Sea experiments, *J. Acoust. Soc. Am.*, 134, 3359–3375.

A Spectra Results

This appendix provides the actual spectral characterizations of the small-scale vertical strain perturbations induced by internal waves and spice for all the appropriate single CTD casts in the LOAPEX, PhilSea09, and PhilSea10 experiments.

In all figures the solid curve is density strain spectrum, dashed is sound speed strain spectrum, and dot-dashed is the cross spectrum.

1.1 LOAPEX Strain Spectra

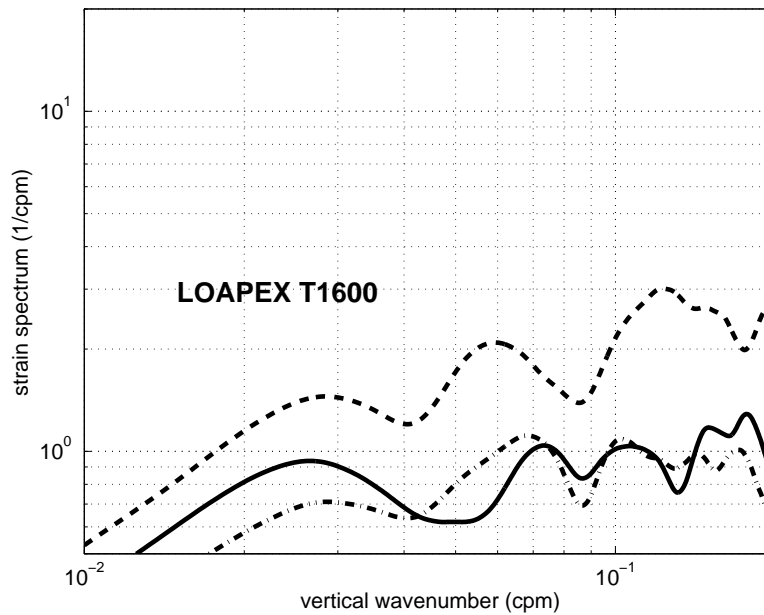


Figure 18: LOAPEX T1600.

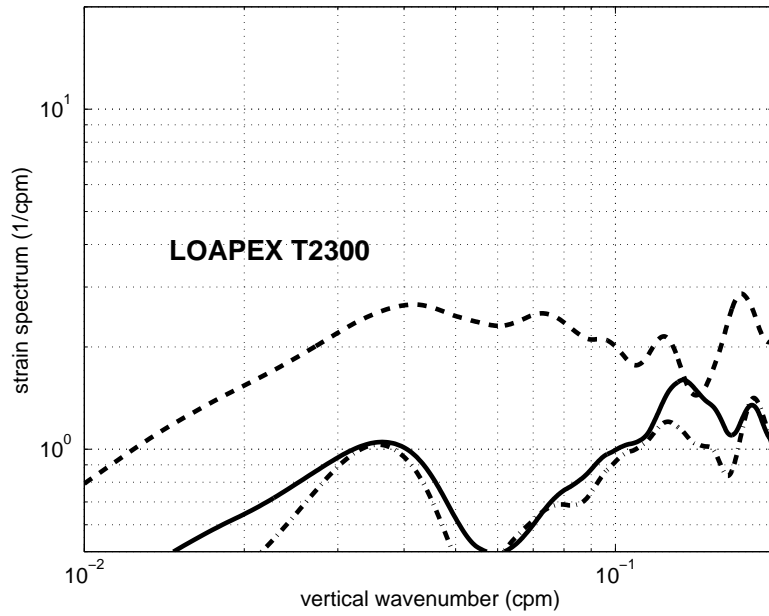


Figure 19: LOAPEX T2300.

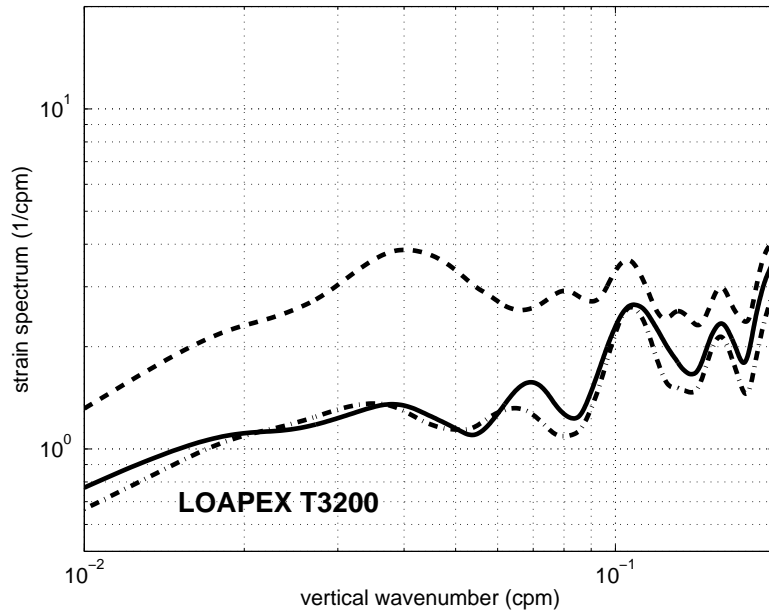


Figure 20: LOAPEX T3200.

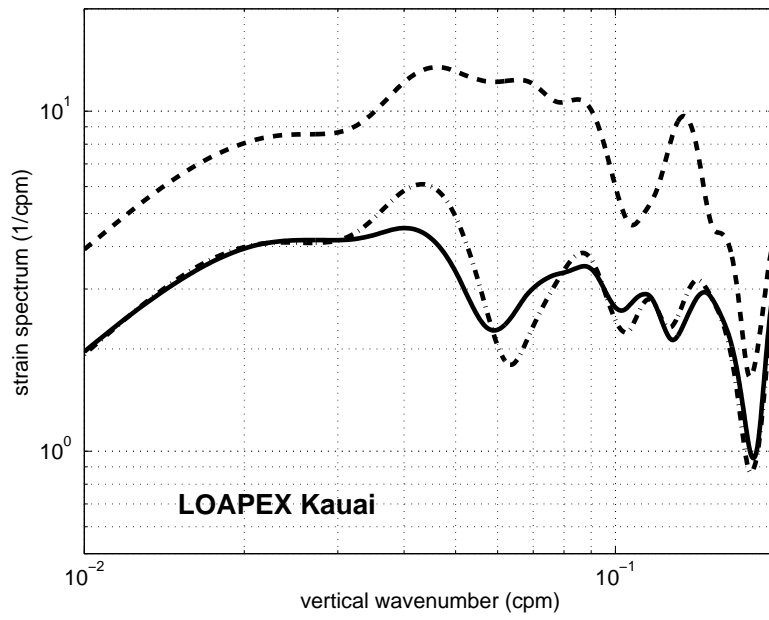


Figure 21: LOAPEX Kauai station.

1.2 PhilSea09 Strain Spectra

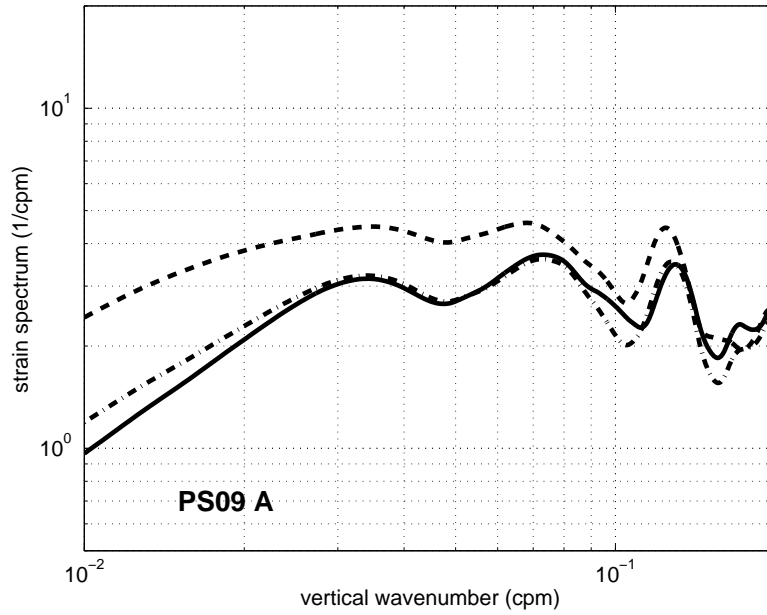


Figure 22: PhilSea09 CTD station A.

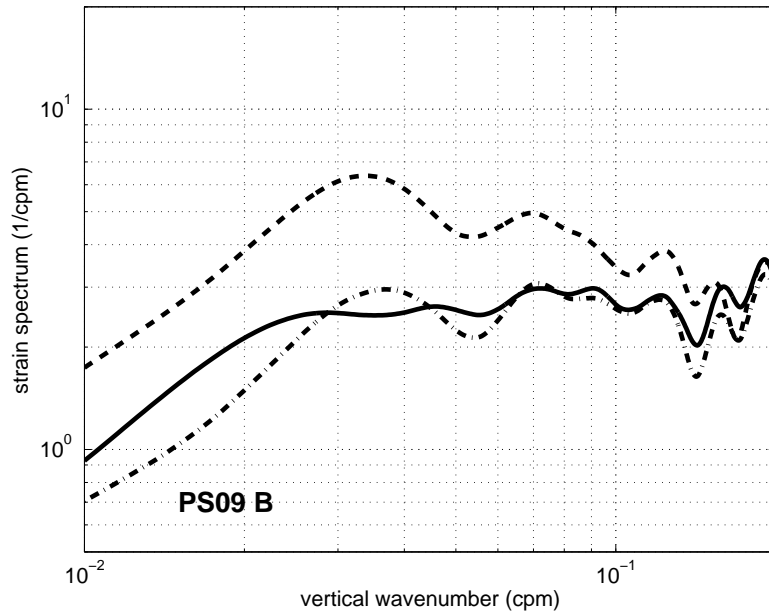


Figure 23: PhilSea09 CTD station B.

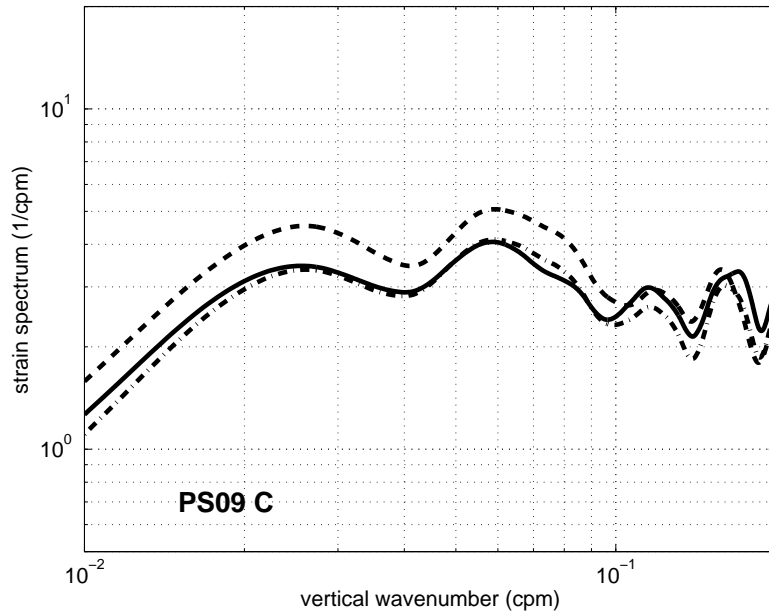


Figure 24: PhilSea09 CTD station C.

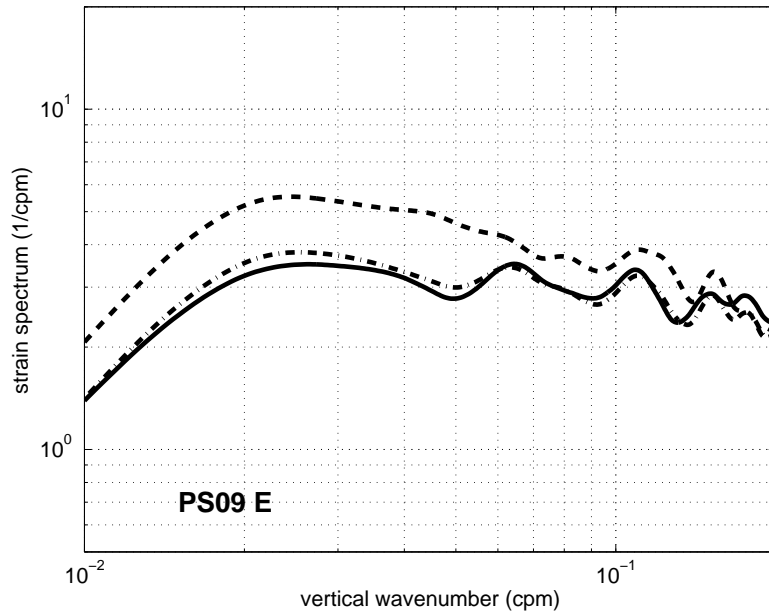


Figure 25: PhilSea09 CTD station E.

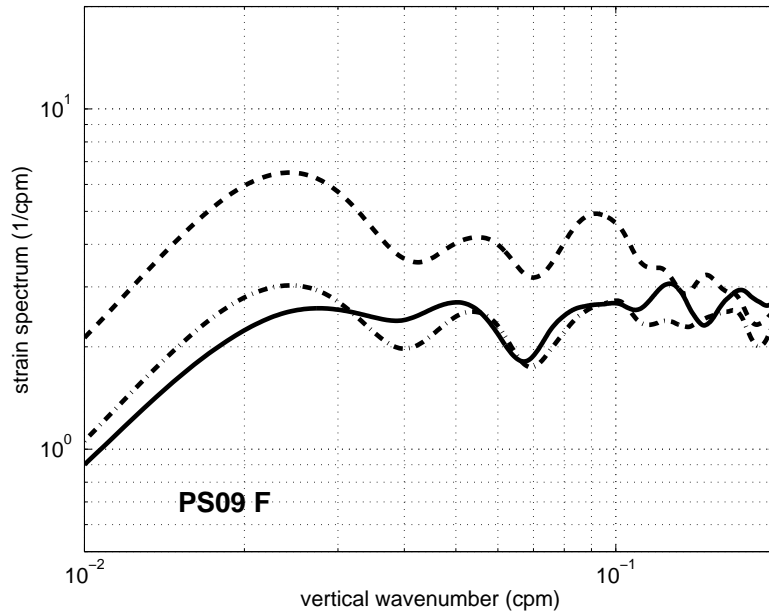


Figure 26: PhilSea09 CTD station F.

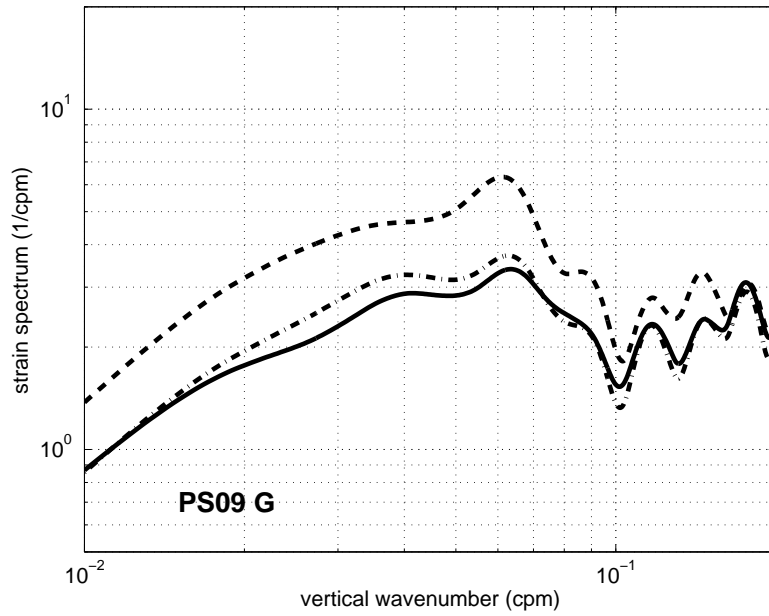


Figure 27: PhilSea09 CTD station G.

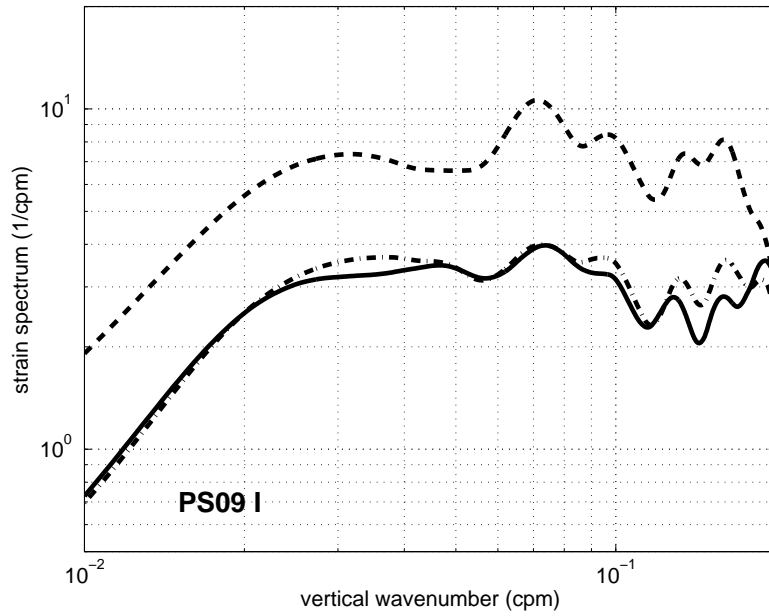


Figure 28: PhilSea09 CTD station I.

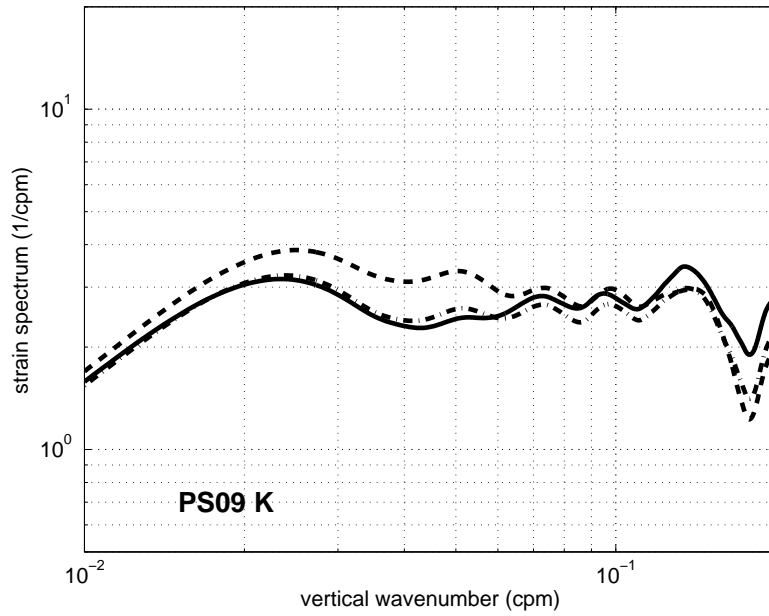


Figure 29: PhilSea09 CTD station K.

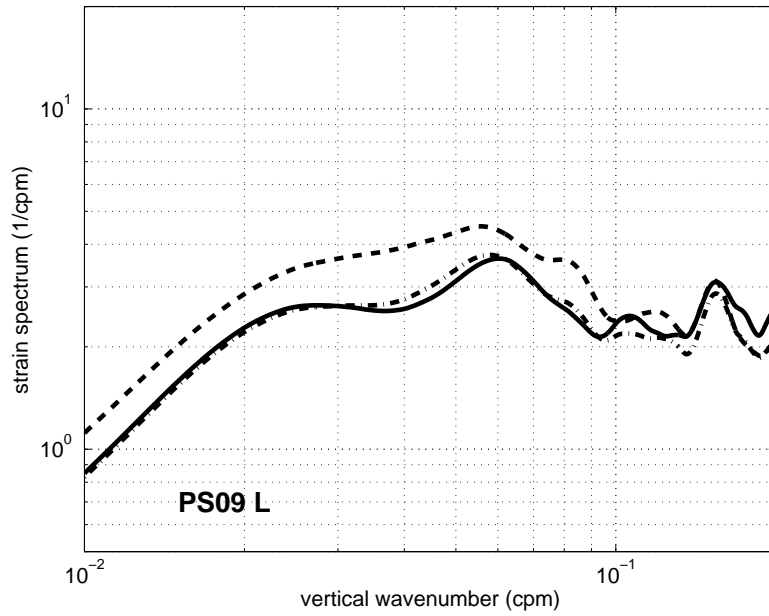


Figure 30: PhilSea09 CTD station L.

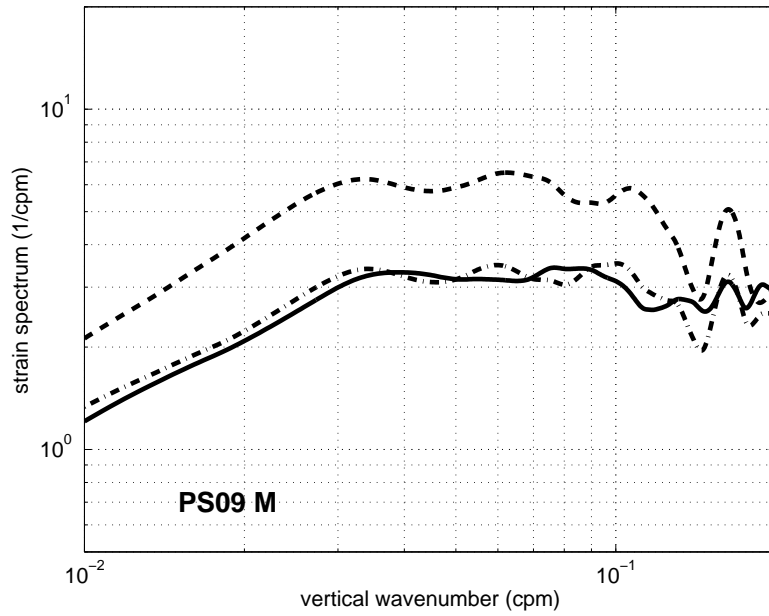


Figure 31: PhilSea09 CTD station M.

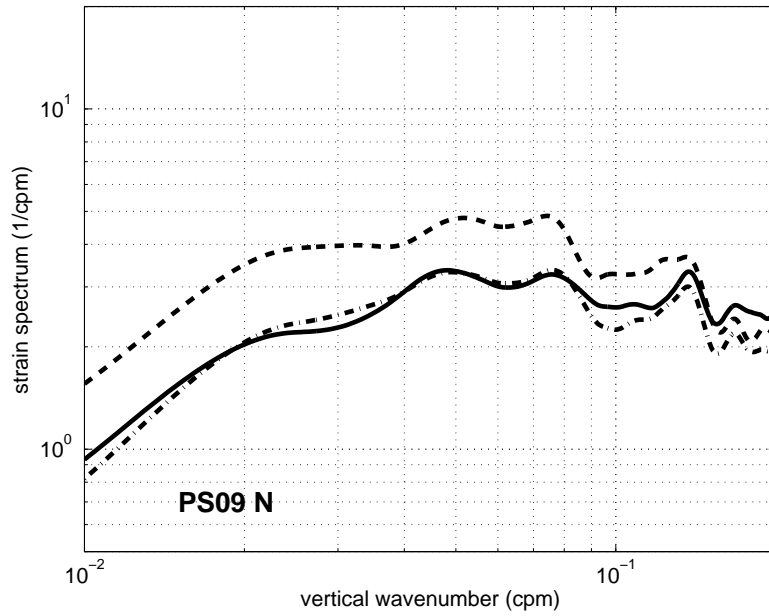


Figure 32: PhilSea09 CTD station N.

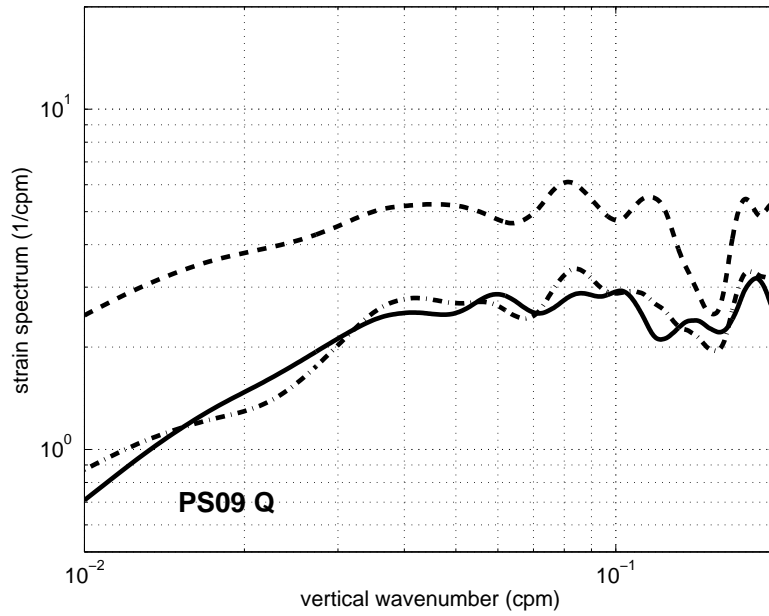


Figure 33: PhilSea09 CTD station Q.

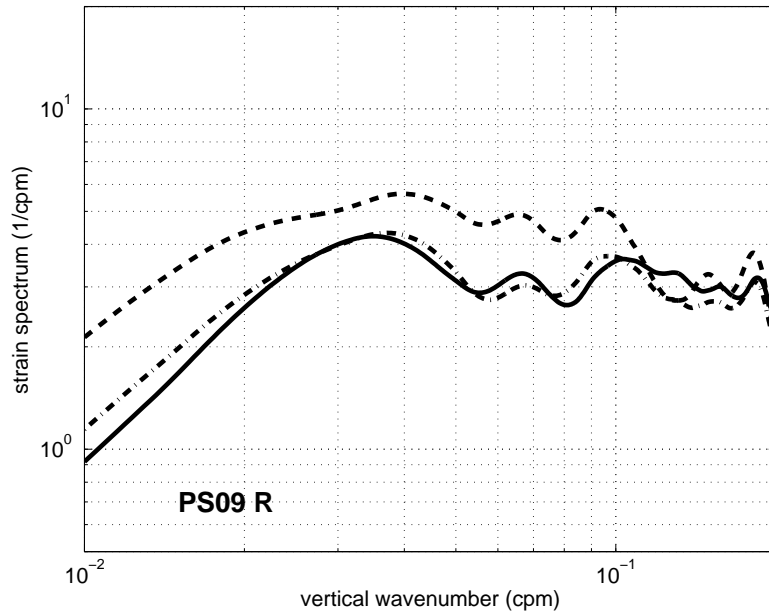


Figure 34: PhilSea09 CTD station R.

1.3 PhilSea10 Strain Spectra

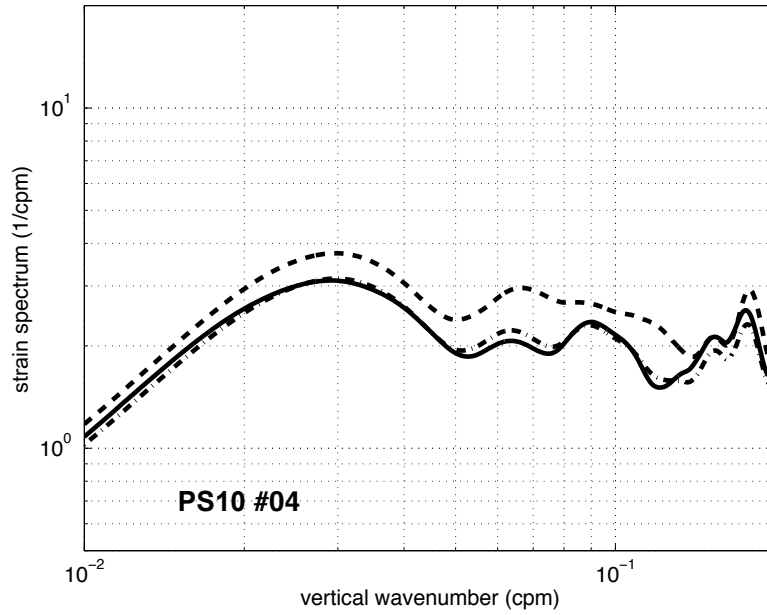


Figure 35: PhilSea10 cast dRR1006_004.

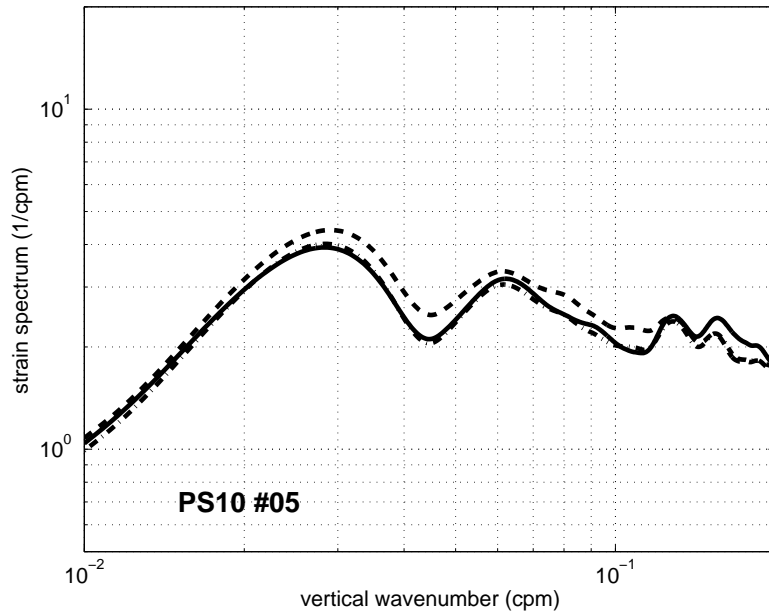


Figure 36: PhilSea10 cast dRR1006_005.

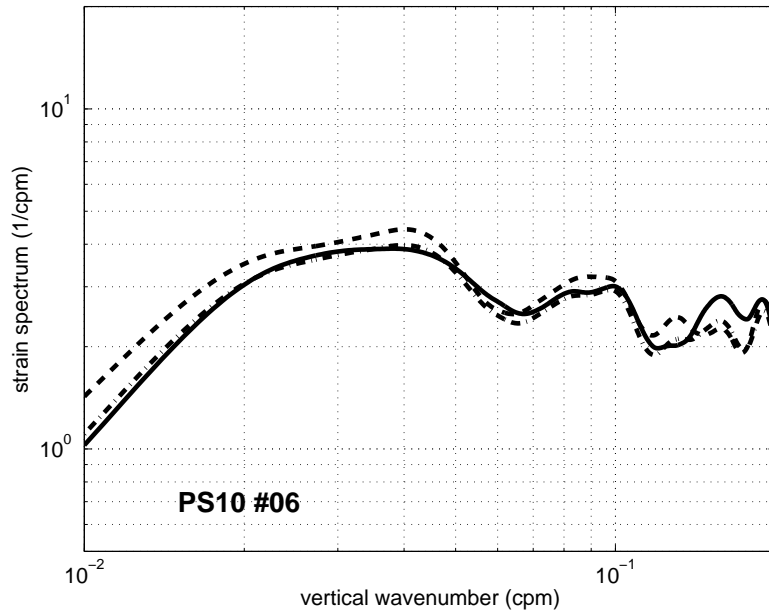


Figure 37: PhilSea10 cast dRR1006_006.

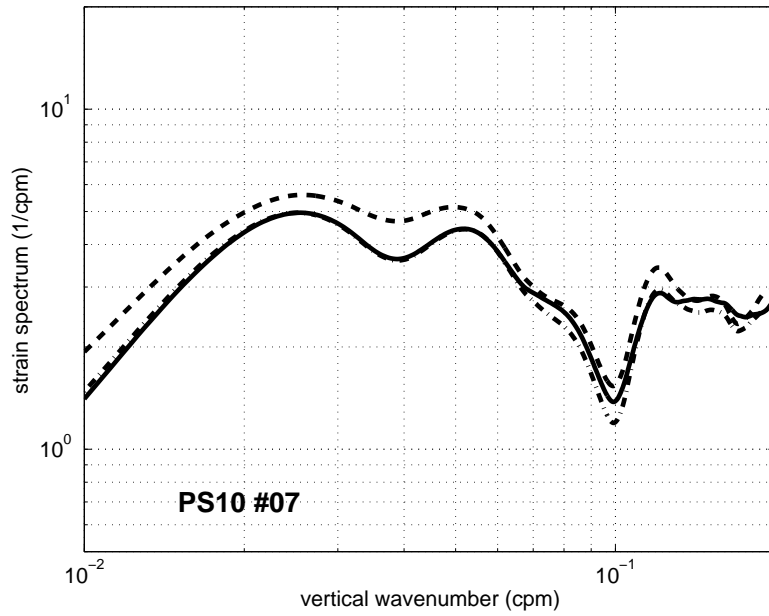


Figure 38: PhilSea10 cast dRR1006_007.

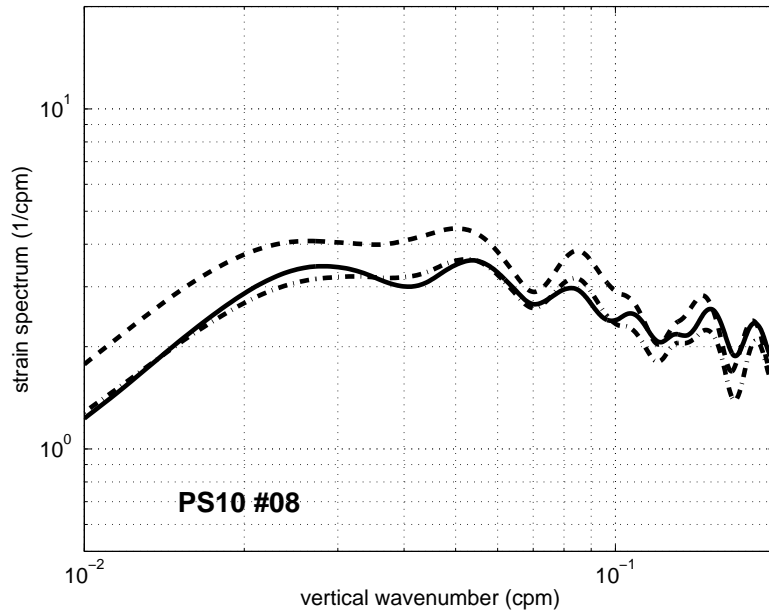


Figure 39: PhilSea10 cast dRR1006_008.

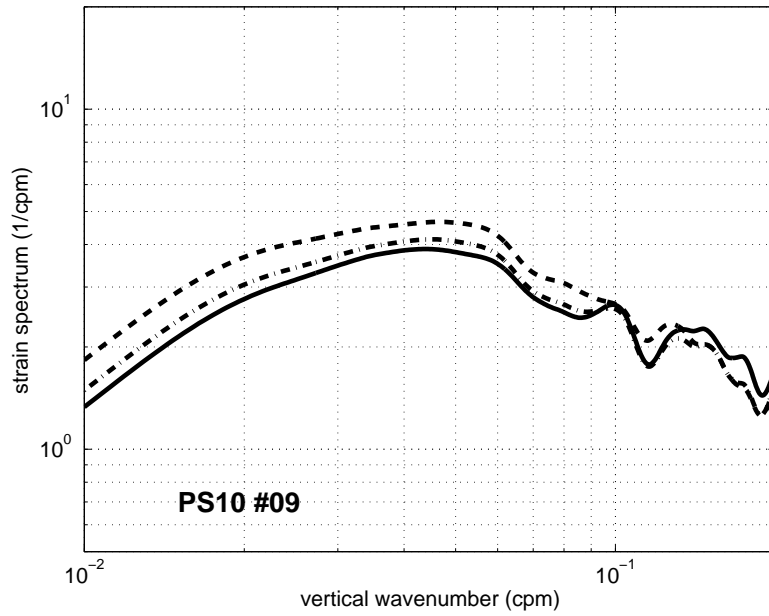


Figure 40: PhilSea10 cast dRR1006_009.

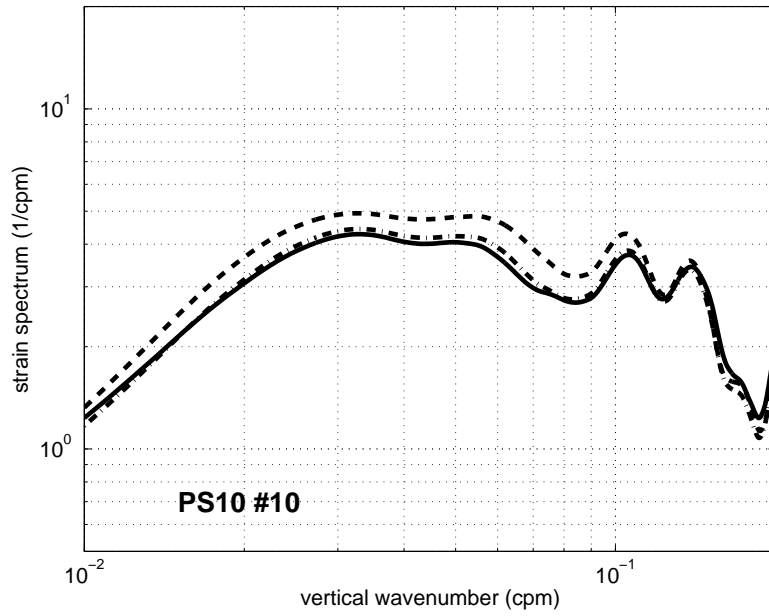


Figure 41: PhilSea10 cast dRR1006_010.

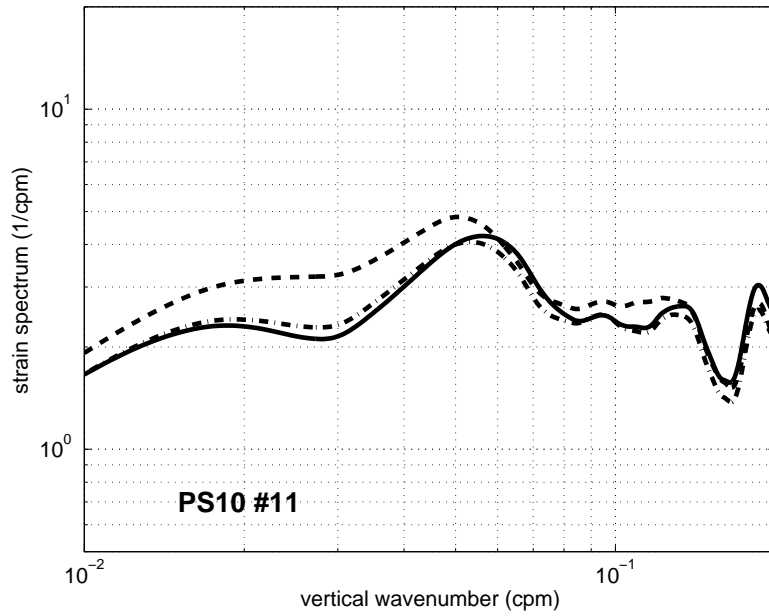


Figure 42: PhilSea10 cast dRR1006_011.

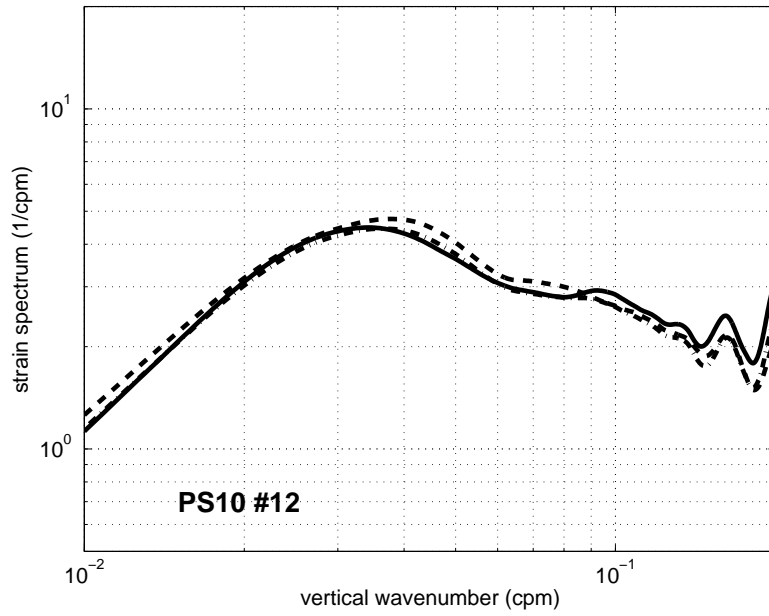


Figure 43: PhilSea10 cast dRR1006_012.

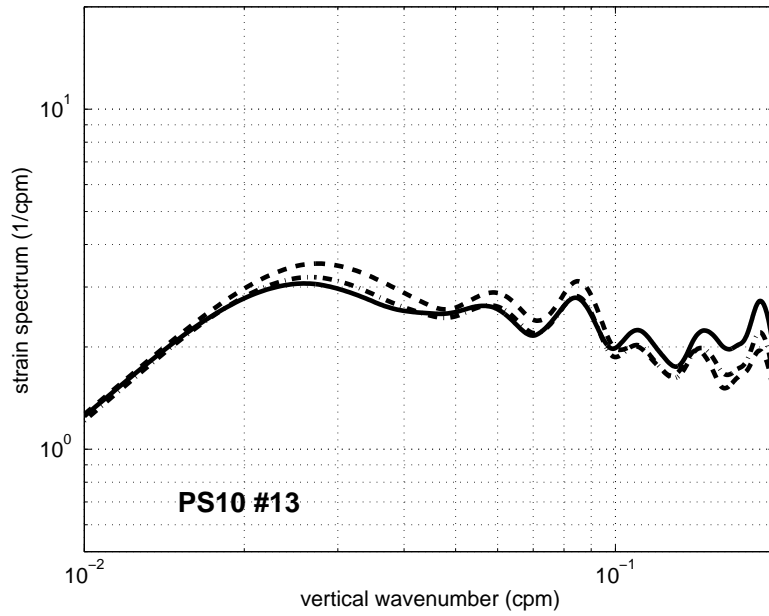


Figure 44: PhilSea10 cast dRR1006_013.

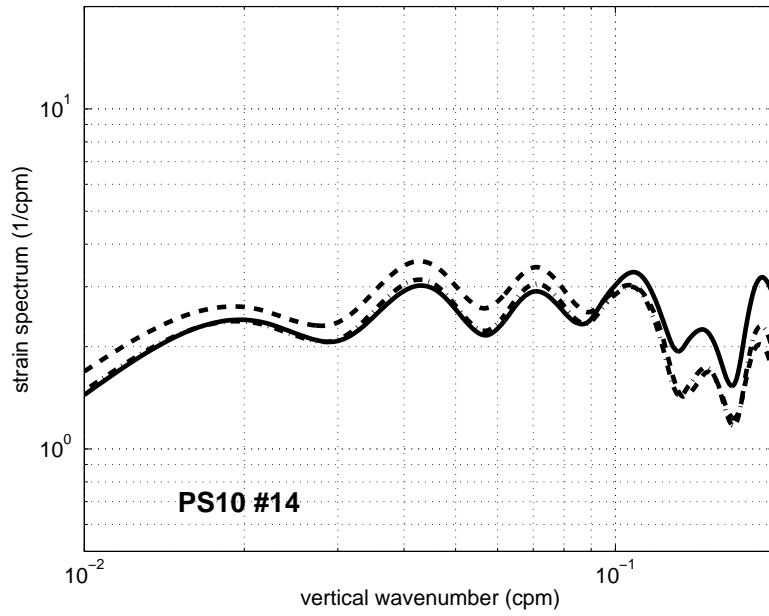


Figure 45: PhilSea10 cast dRR1006_014.

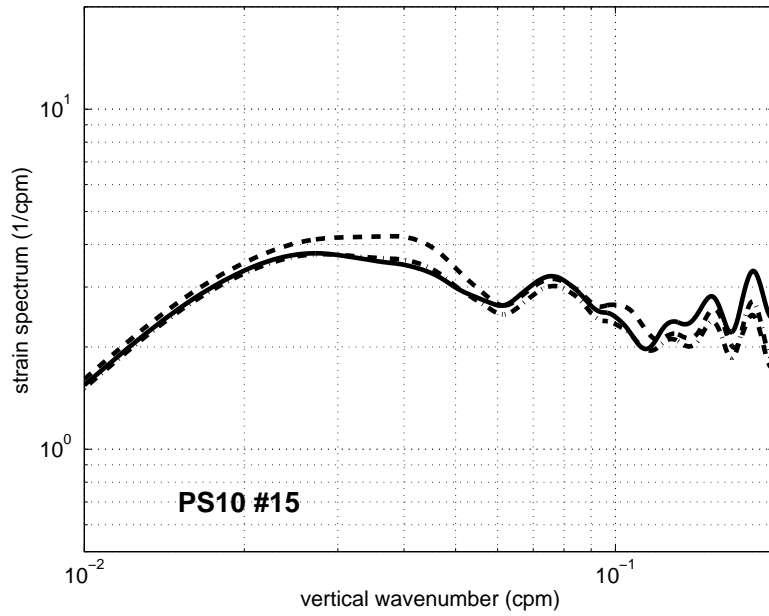


Figure 46: PhilSea10 cast dRR1006_015.

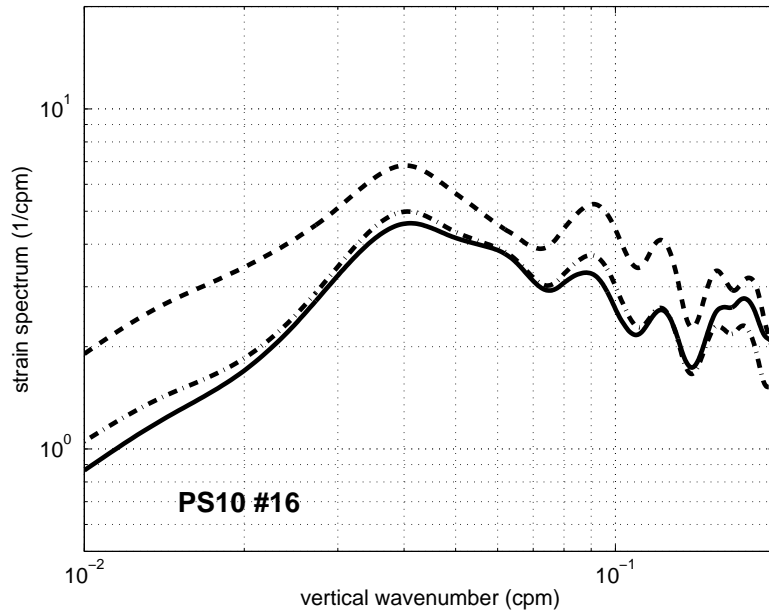


Figure 47: PhilSea10 cast dRR1006_016.

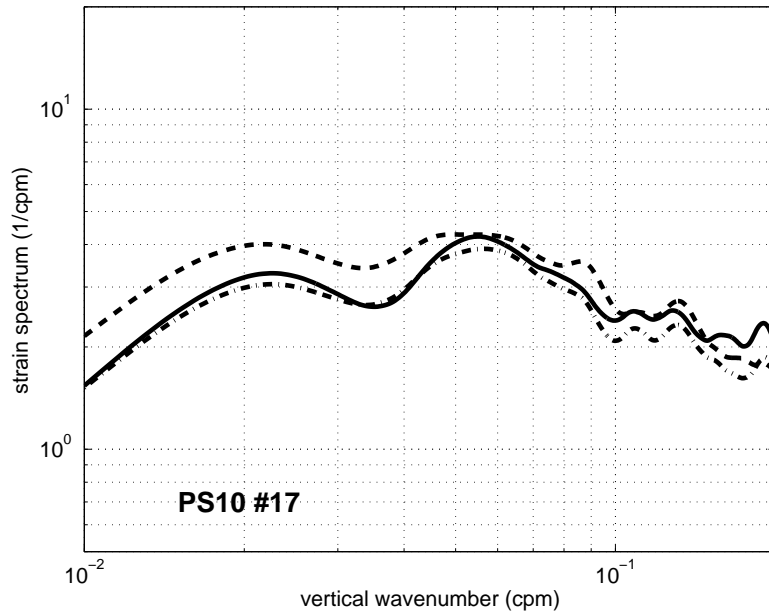


Figure 48: PhilSea10 cast dRR1006_017.

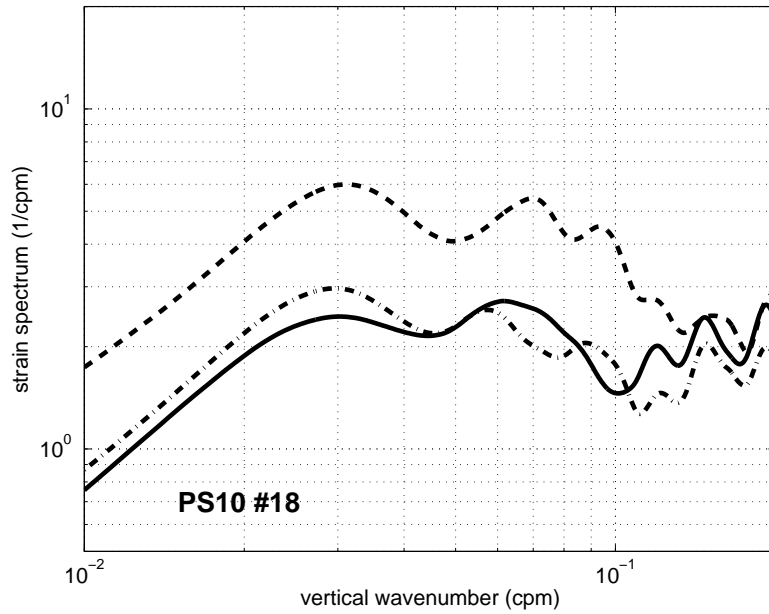


Figure 49: PhilSea10 cast dRR1006_018.

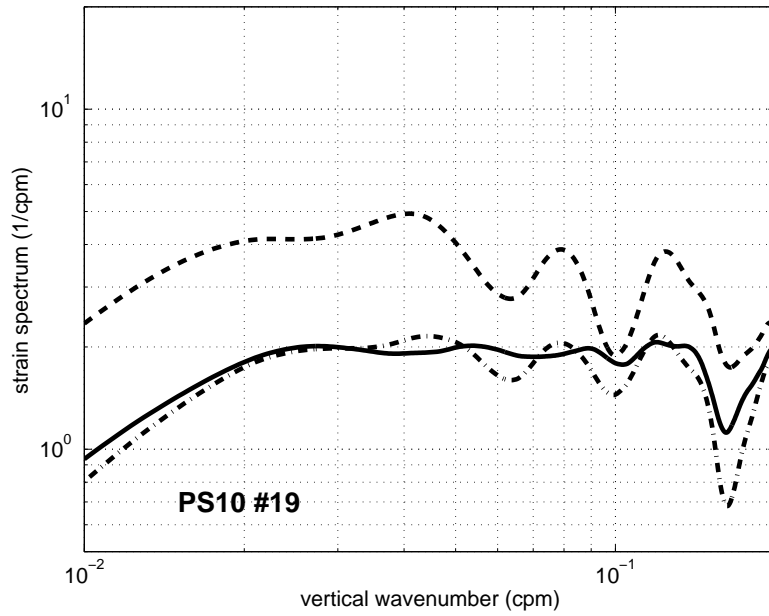


Figure 50: PhilSea10 cast dRR1006_019.

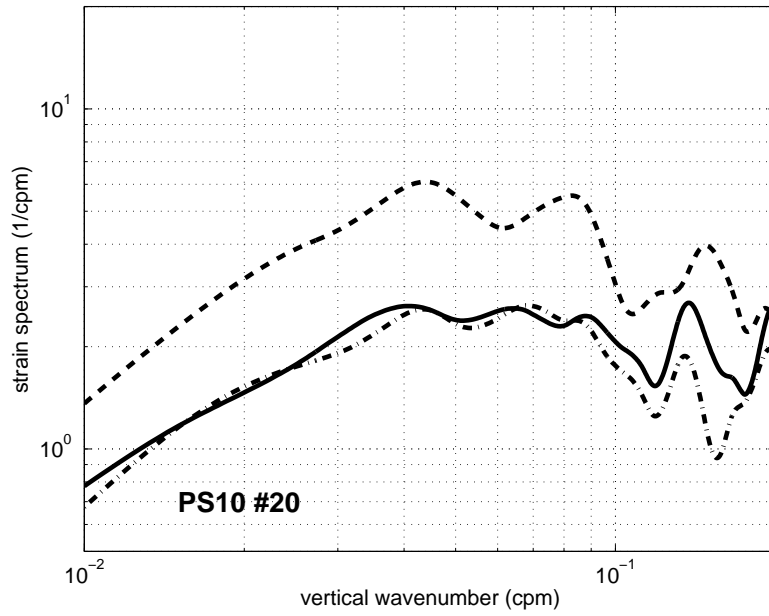


Figure 51: PhilSea10 cast dRR1006_020.

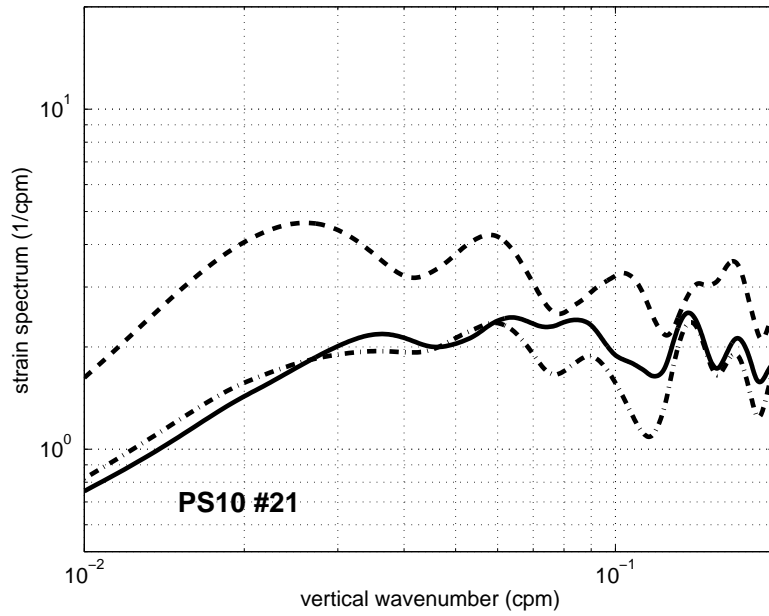


Figure 52: PhilSea10 cast dRR1006_021.

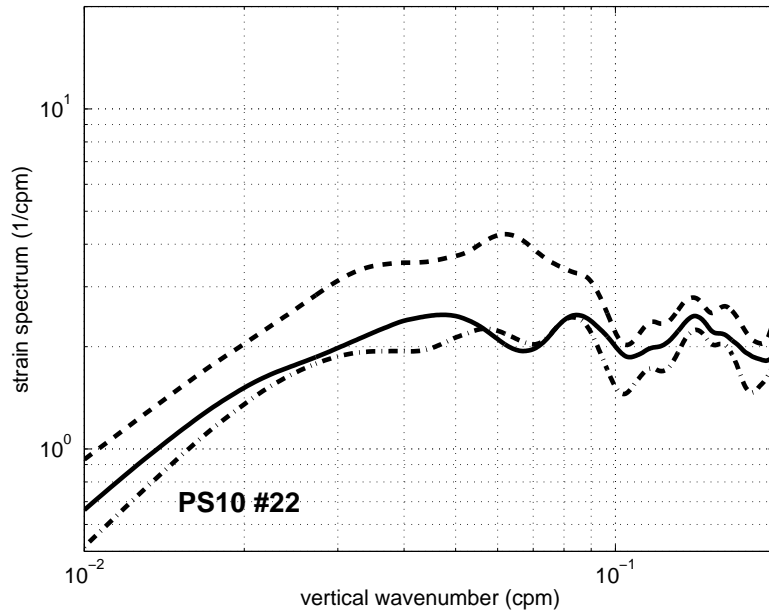


Figure 53: PhilSea10 cast dRR1006_022.

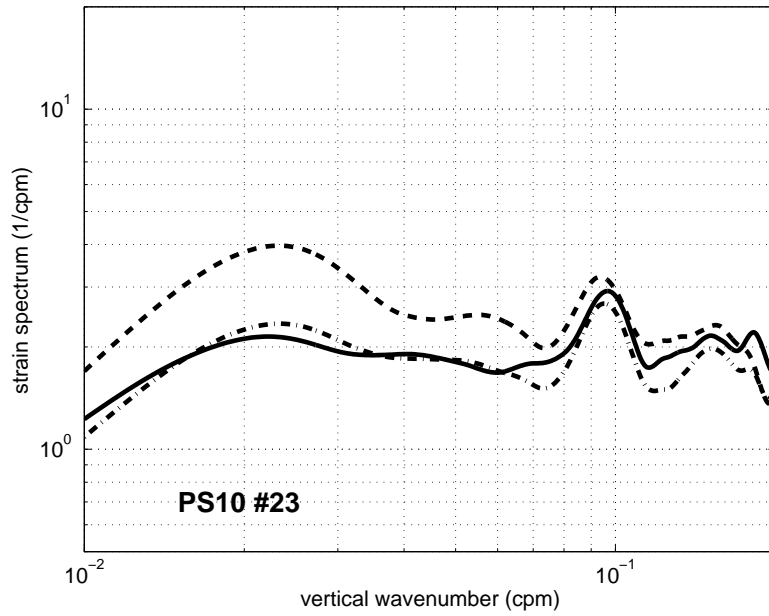


Figure 54: PhilSea10 cast dRR1006_023.

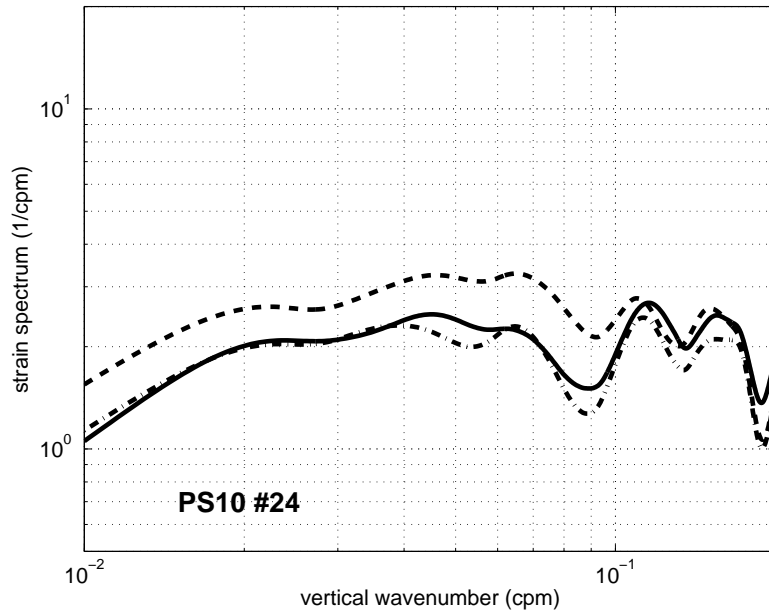


Figure 55: PhilSea10 cast dRR1006_024.

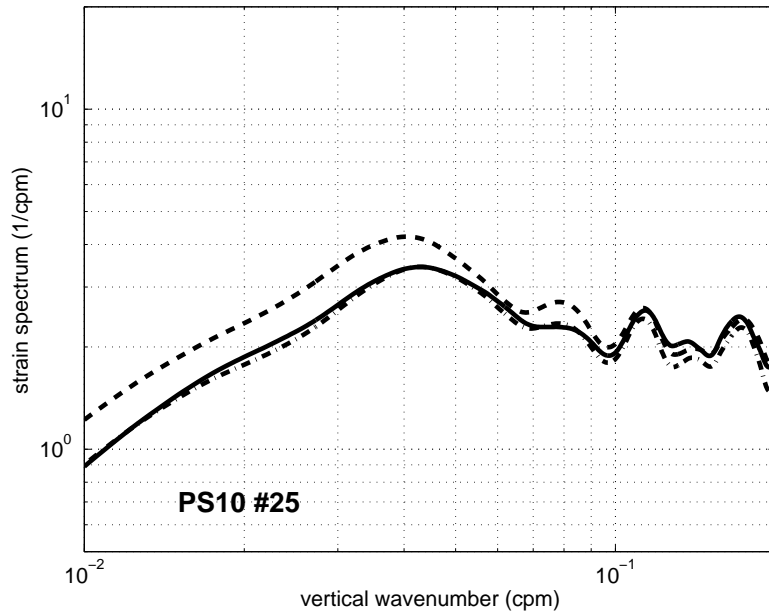


Figure 56: PhilSea10 cast dRR1006_025.

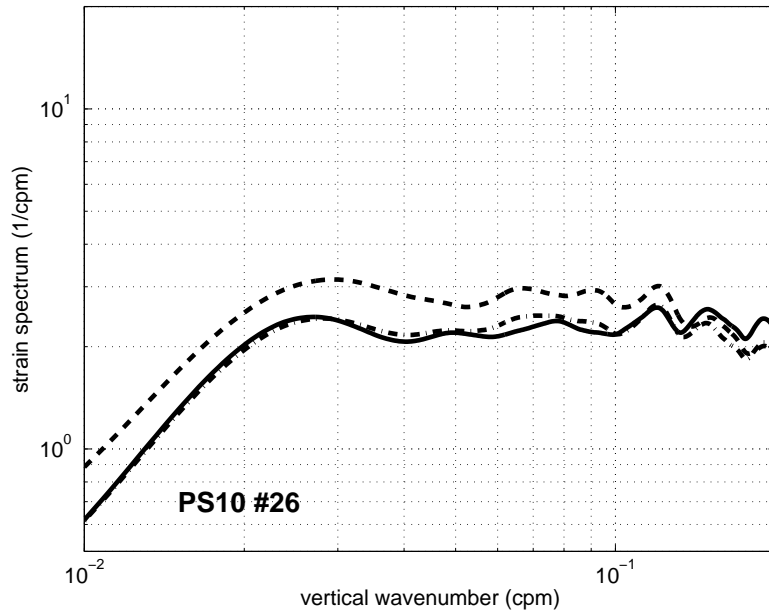


Figure 57: PhilSea10 cast dRR1006_026.

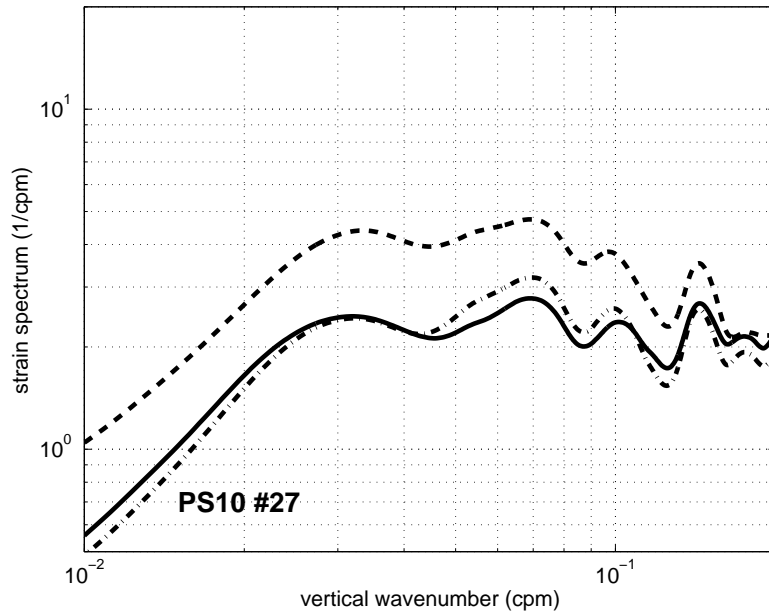


Figure 58: PhilSea10 cast dRR1006_027.

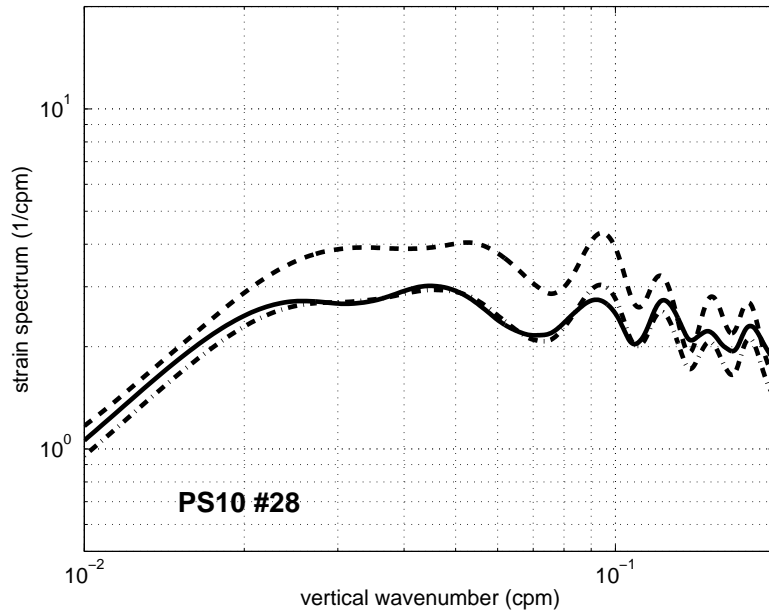


Figure 59: PhilSea10 cast dRR1006_028.

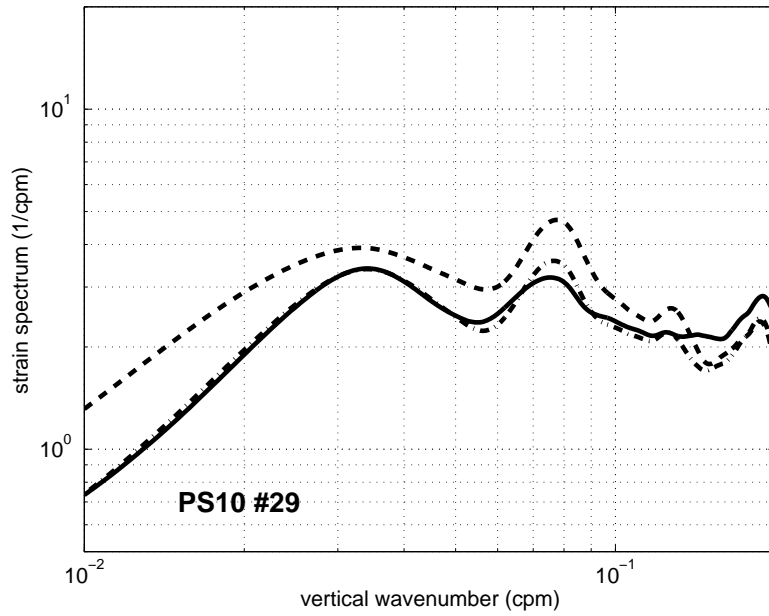


Figure 60: PhilSea10 cast dRR1006_029.

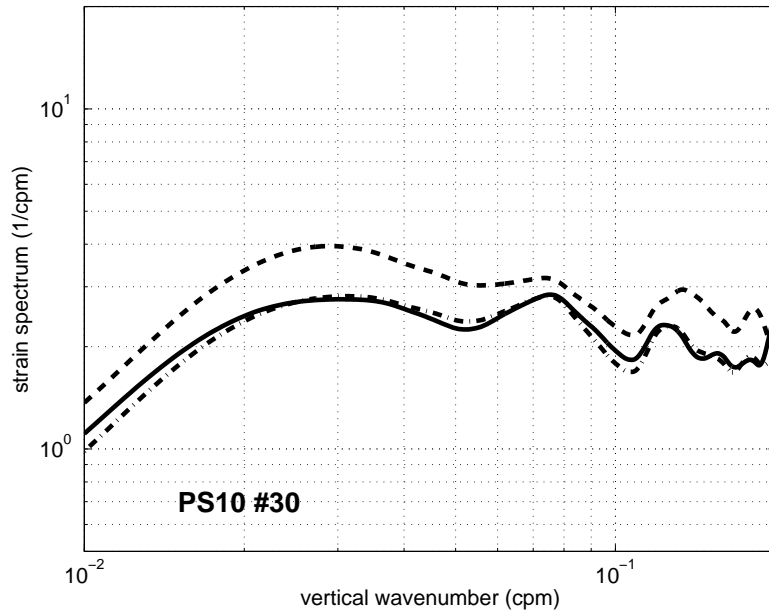


Figure 61: PhilSea10 cast dRR1006_030.

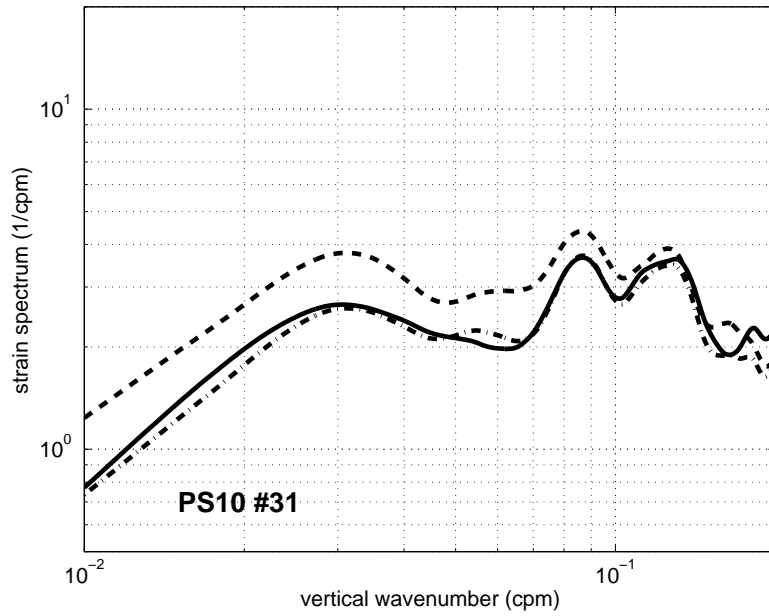


Figure 62: PhilSea10 cast dRR1006_031.

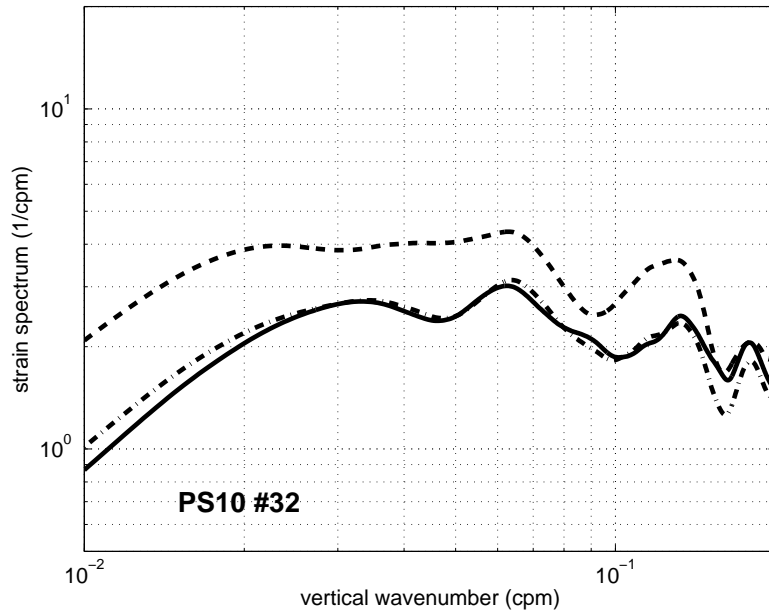


Figure 63: PhilSea10 cast dRR1006_032.

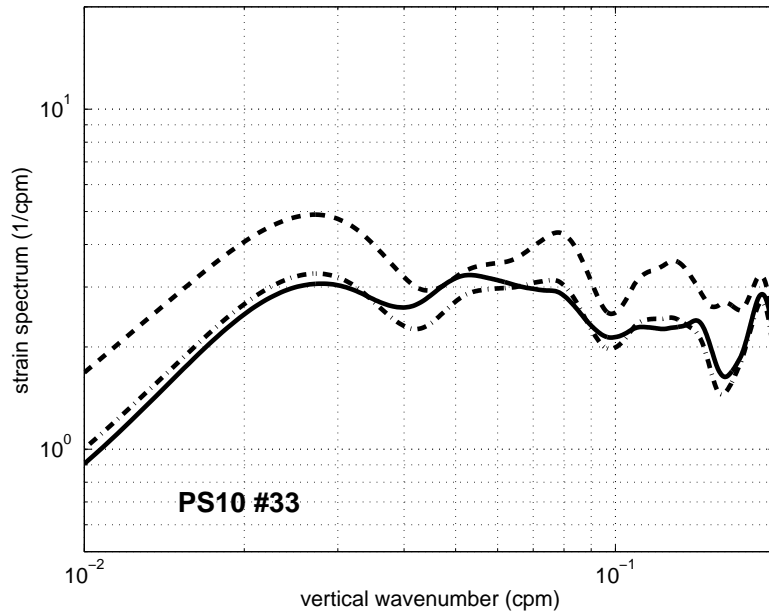


Figure 64: PhilSea10 cast dRR1006_033.

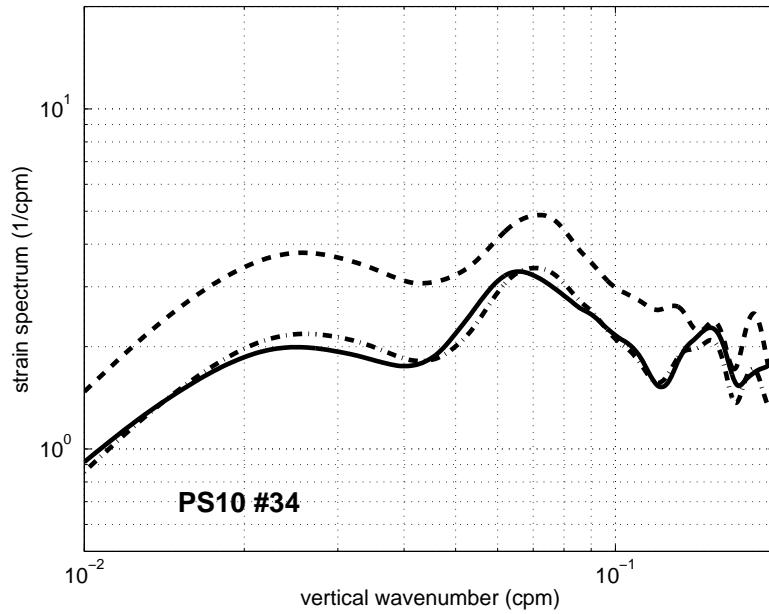


Figure 65: PhilSea10 cast dRR1006_034.

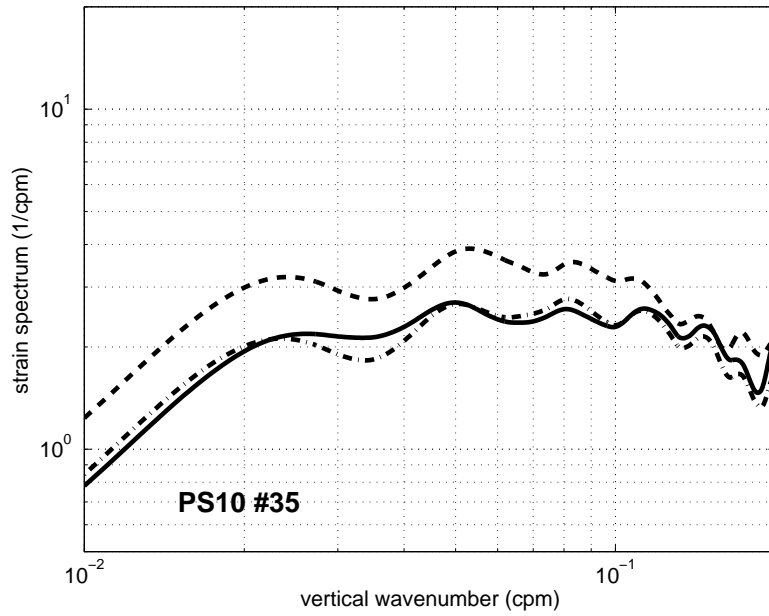


Figure 66: PhilSea10 cast dRR1006_035.

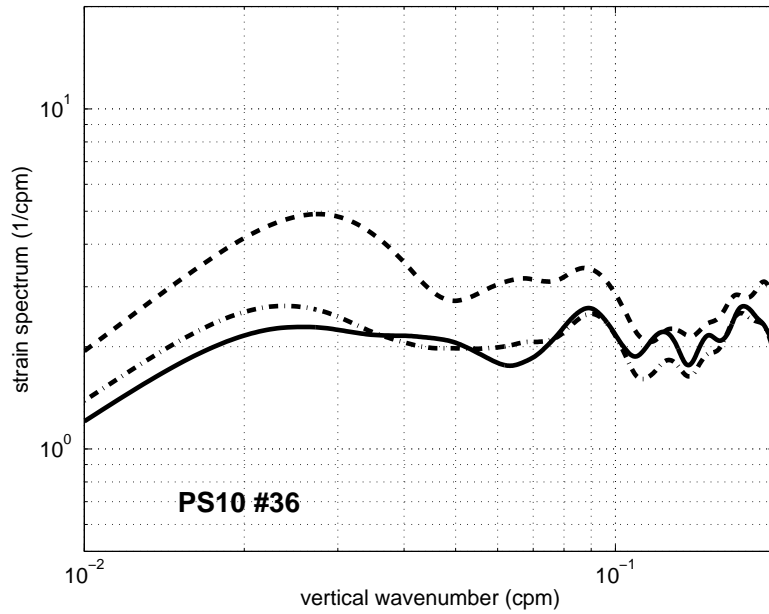


Figure 67: PhilSea10 cast dRR1006_036.

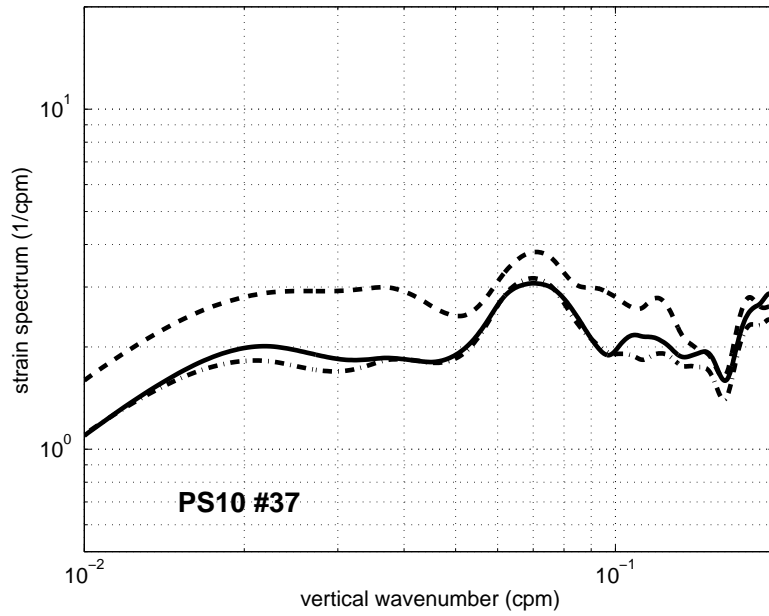


Figure 68: PhilSea10 cast dRR1006_037.

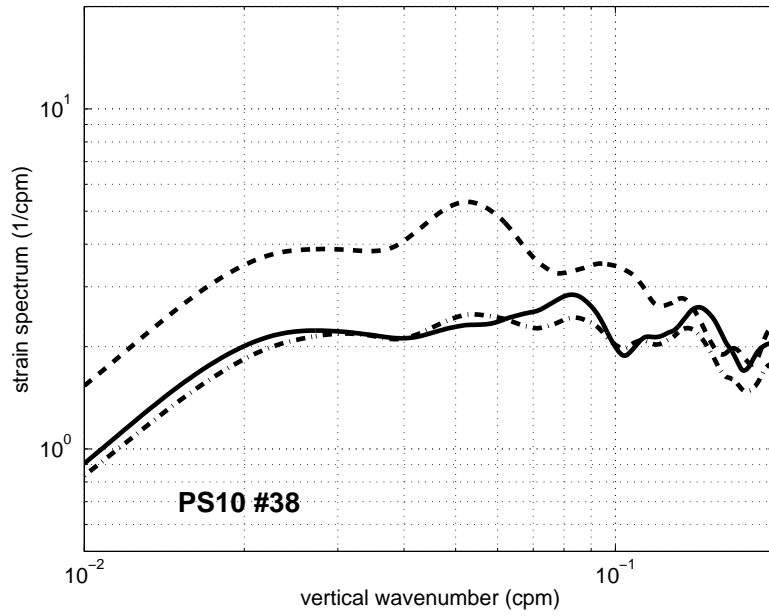


Figure 69: PhilSea10 cast dRR1006_038.

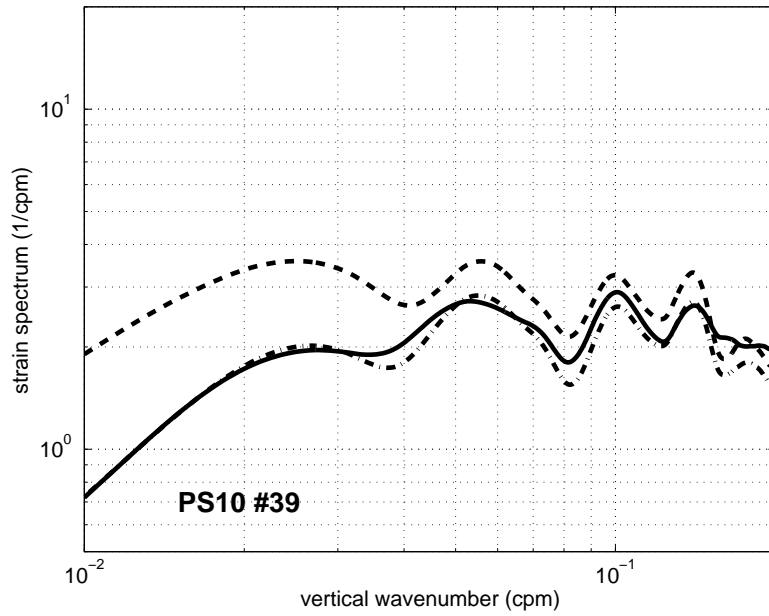


Figure 70: PhilSea10 cast dRR1006_039.

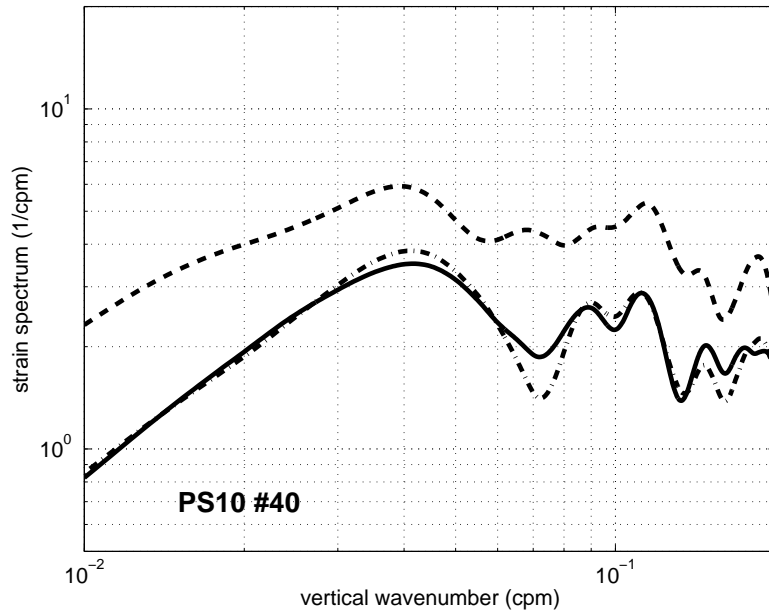


Figure 71: PhilSea10 cast dRR1006_040.

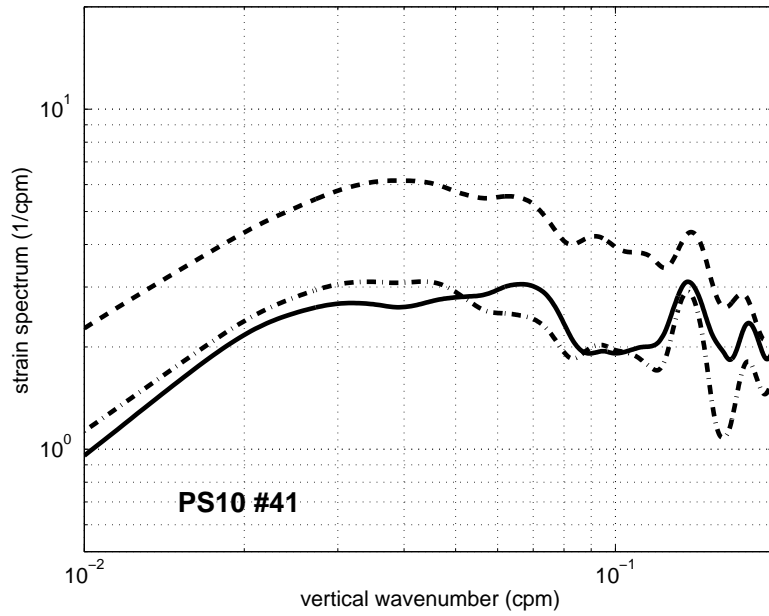


Figure 72: PhilSea10 cast dRR1006_041.

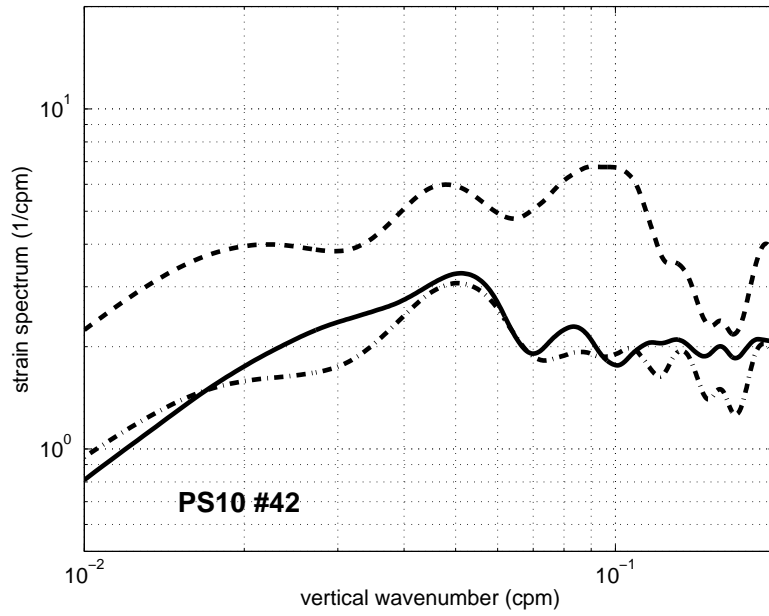


Figure 73: PhilSea10 cast dRR1006_042.

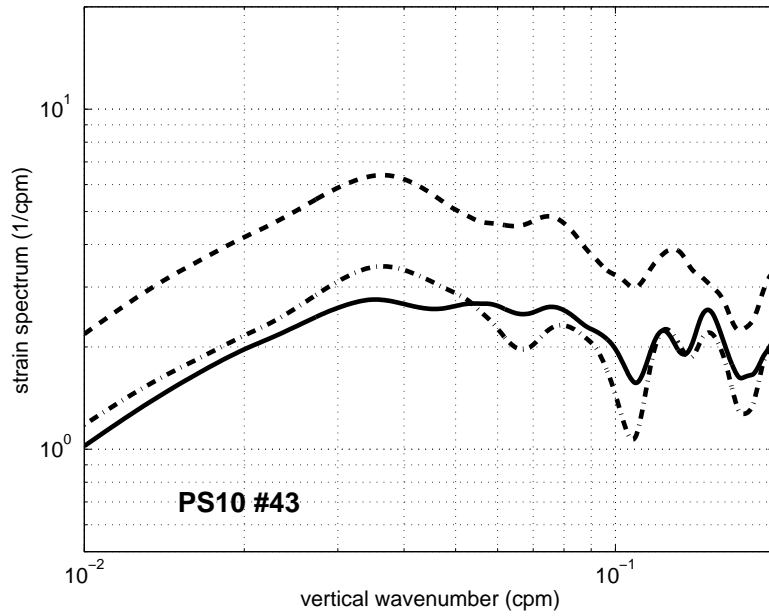


Figure 74: PhilSea10 cast dRR1006_043.

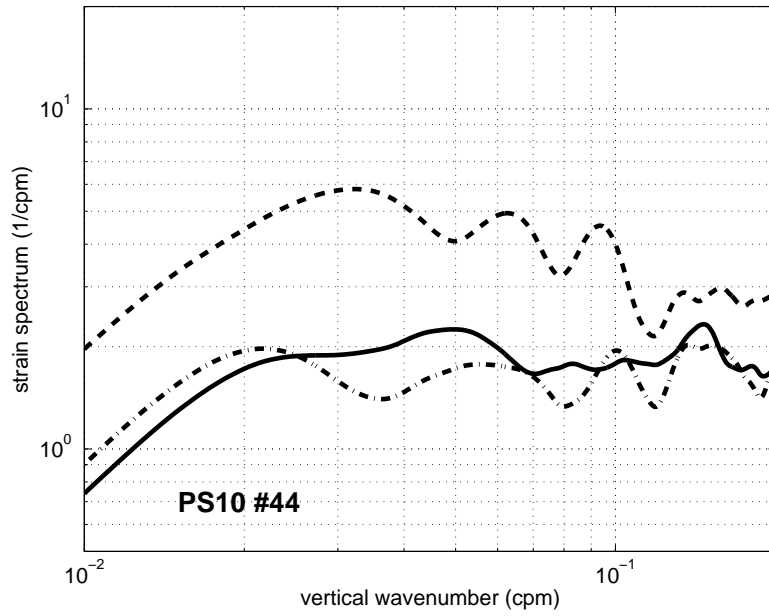


Figure 75: PhilSea10 cast dRR1006_044.

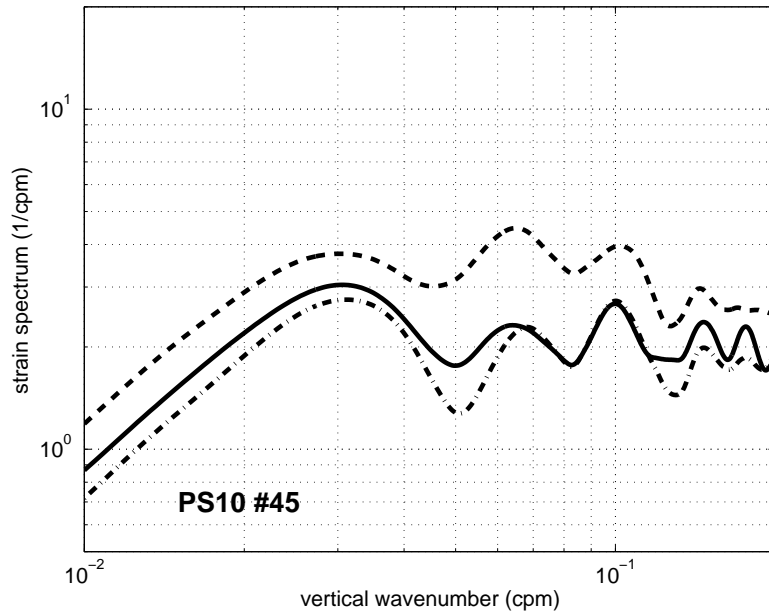


Figure 76: PhilSea10 cast dRR1006_045.

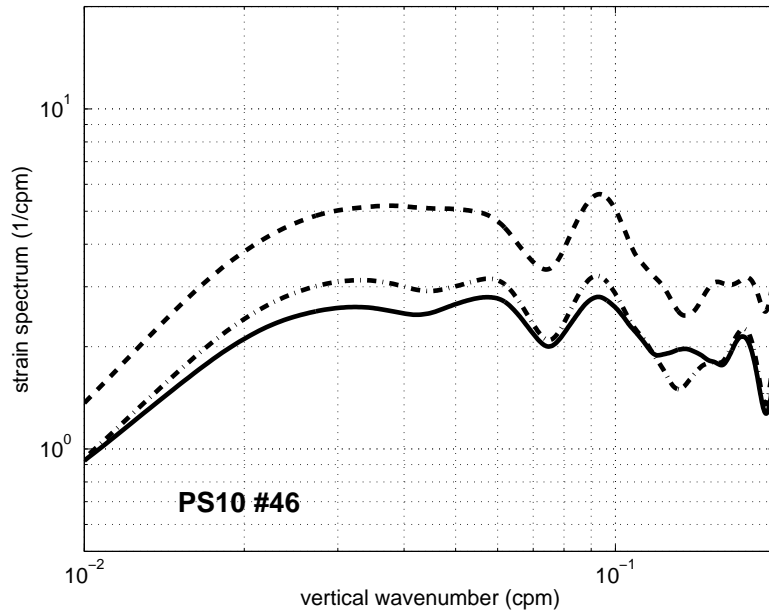


Figure 77: PhilSea10 cast dRR1006_046.

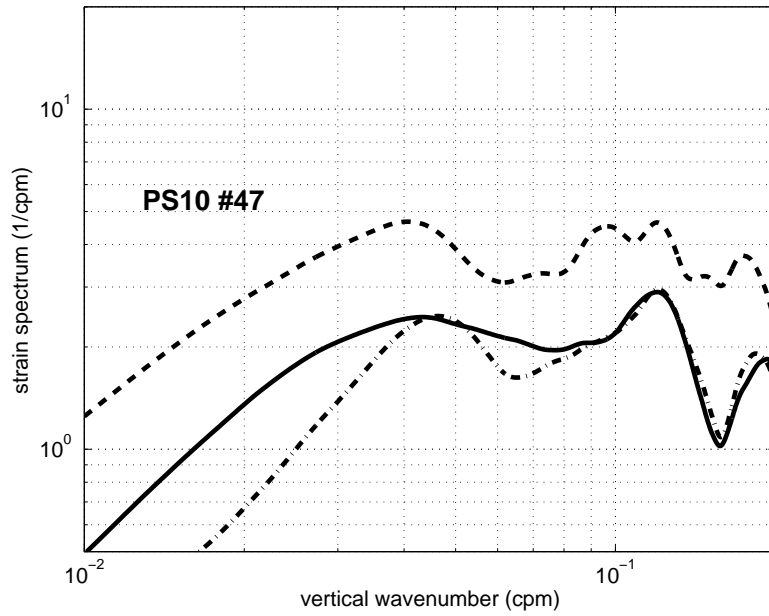


Figure 78: PhilSea10 cast dRR1006_047.

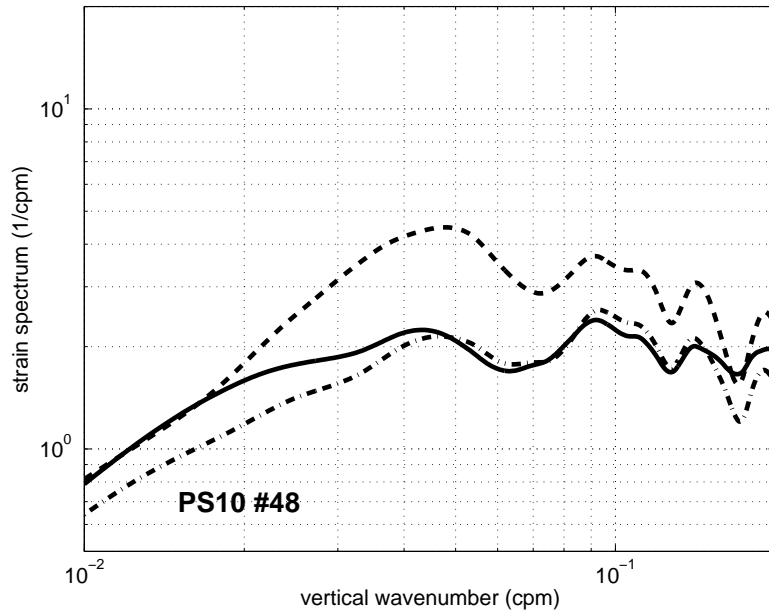


Figure 79: PhilSea10 cast dRR1006_048.

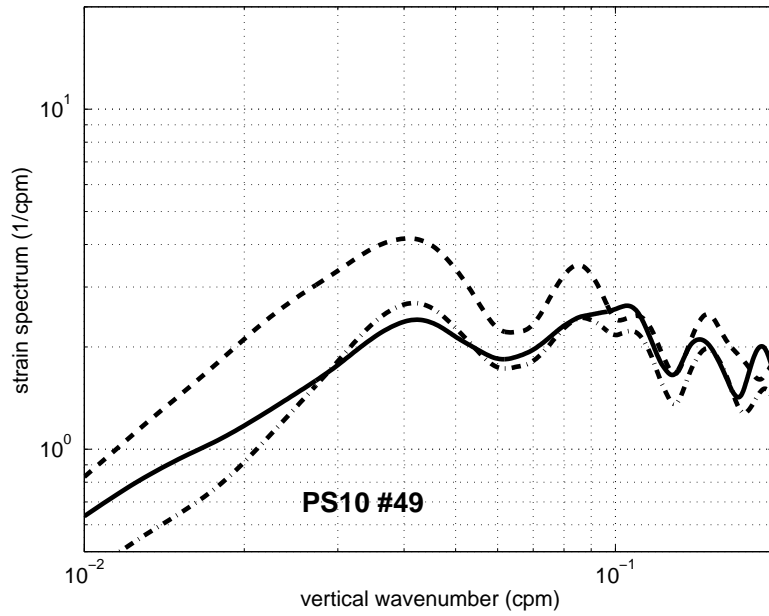


Figure 80: PhilSea10 cast dRR1006_049.

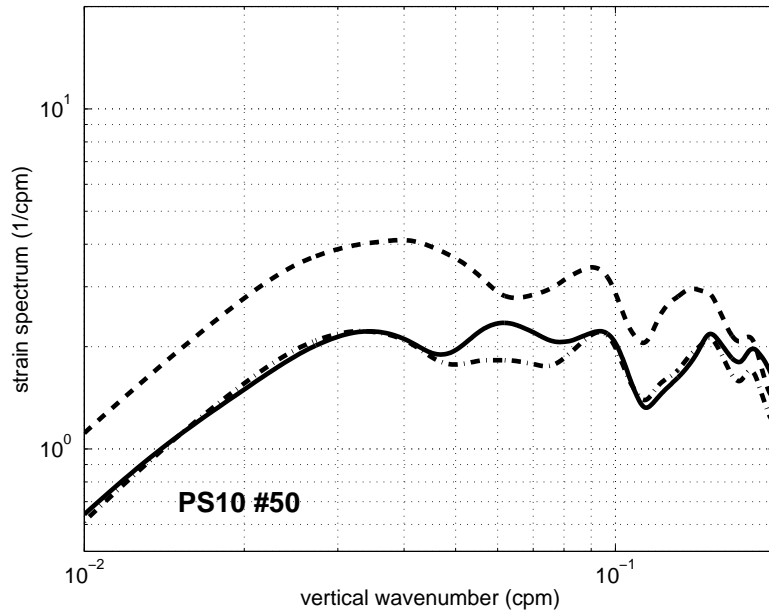


Figure 81: PhilSea10 cast dRR1006_050.

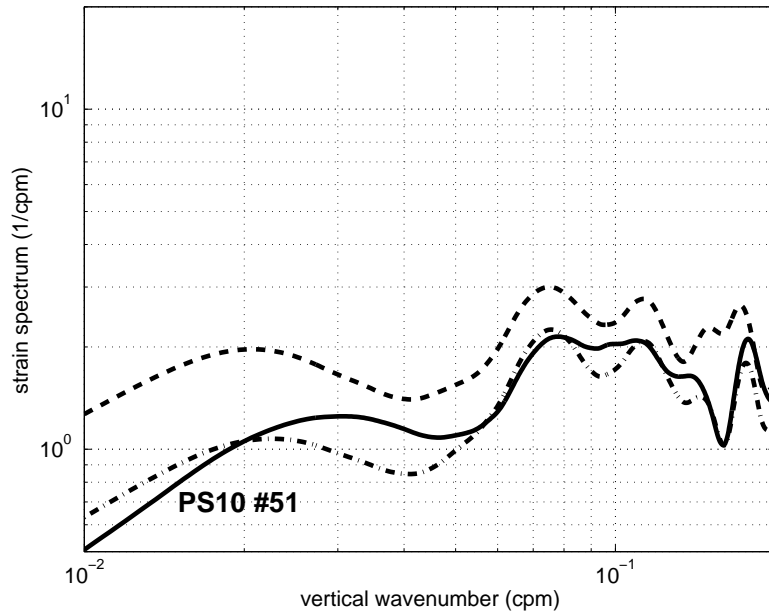


Figure 82: PhilSea10 cast dRR1006_051.

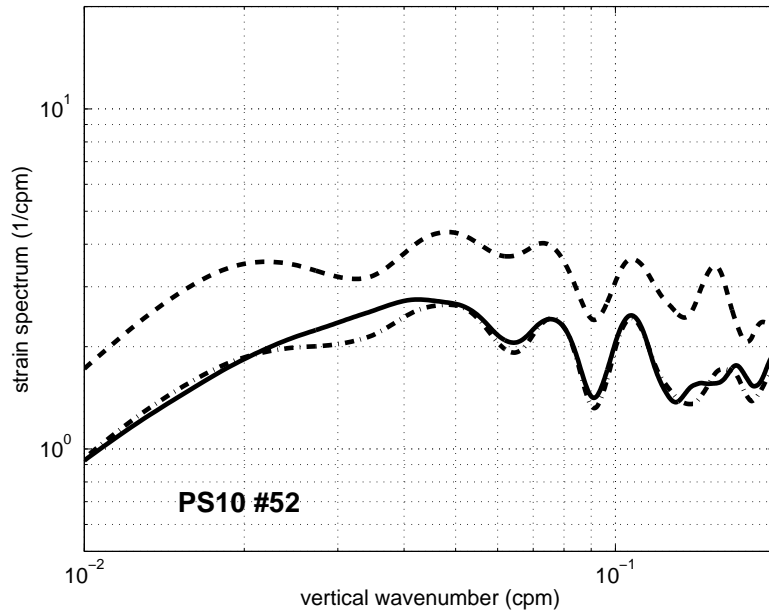


Figure 83: PhilSea10 cast dRR1006_052.

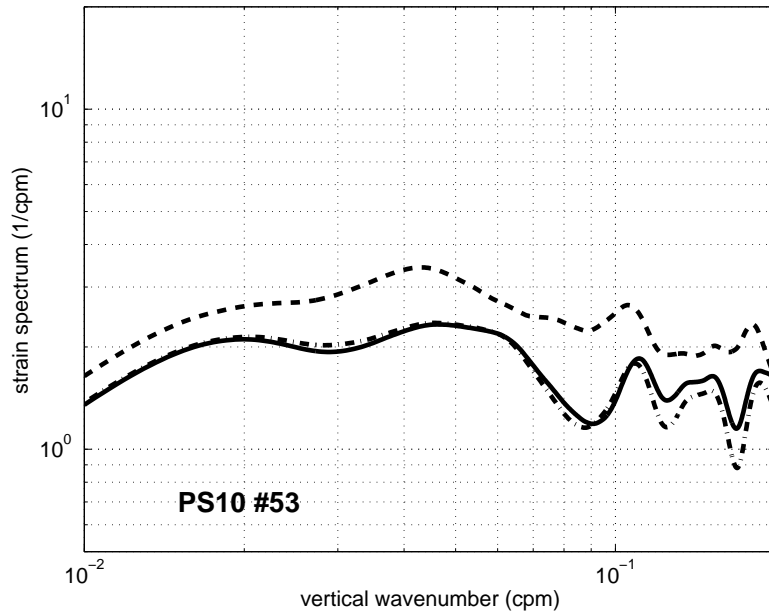


Figure 84: PhilSea10 cast dRR1006_053.

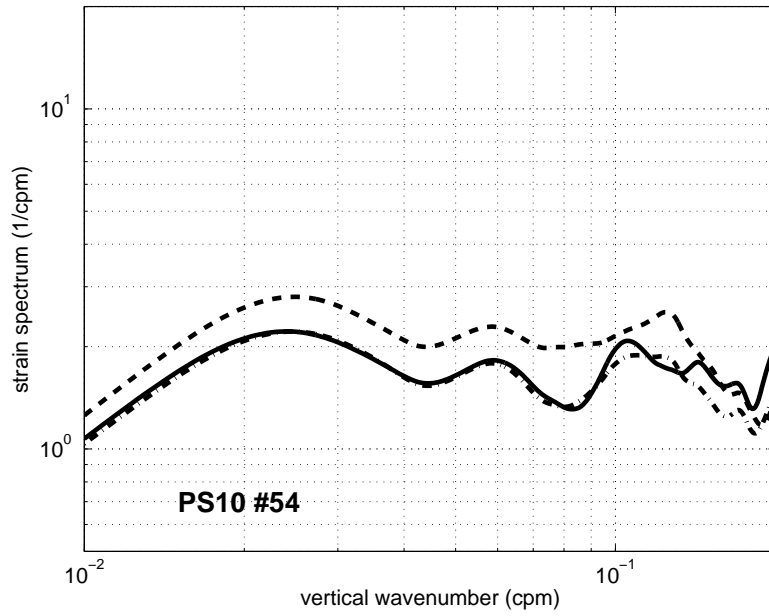


Figure 85: PhilSea10 cast dRR1006_054.

REPORT DOCUMENTATION PAGE

Form Approved
OPM No. 0704-0188

Public reporting burden for this collection of information is estimated to average 1 hour per response, including the time for reviewing instructions, searching existing data sources, gathering and maintaining the data needed, and reviewing the collection of information. Send comments regarding this burden estimate or any other aspect of this collection of information, including suggestions for reducing this burden, to Washington Headquarters Services, Directorate for Information Operations and Reports, 1215 Jefferson Davis Highway, Suite 1204, Arlington, VA 22202-4302, and to the Office of Information and Regulatory Affairs, Office of Management and Budget, Washington, DC 20503.

1. AGENCY USE ONLY (<i>Leave blank</i>)		2. REPORT DATE March 2014	3. REPORT TYPE AND DATES COVERED Technical Memorandum	
4. TITLE AND SUBTITLE A Method to Determine Small-Scale Internal Wave and Spice Fields from a Single CTD Profile with Application to Three Long-Range Ocean Acoustics Experiments			5. FUNDING NUMBERS N00014-03-1-0181 N00014-07-1-0743 N00014-08-1-0843 N00014-06-1-0194 N00014-13-1-0009	
6. AUTHOR(S) F.S. Henyey, J.A. Mercer, R.K. Andrew, and A.W. White				
7. PERFORMING ORGANIZATION NAME(S) AND ADDRESS(ES) Applied Physics Laboratory University of Washington 1013 NE 40th Street Seattle, WA 98105-6698			8. PERFORMING ORGANIZATION REPORT NUMBER APL-UW TM 1-14	
9. SPONSORING / MONITORING AGENCY NAME(S) AND ADDRESS(ES) Dr. Robert Headrick, Code 322OA Office of Naval Research One Liberty Center 875 North Randolph Street, Suite 4125 Arlington, VA 22203			10. SPONSORING / MONITORING AGENCY REPORT NUMBER	
11. SUPPLEMENTARY NOTES				
12a. DISTRIBUTION / AVAILABILITY STATEMENT <i>Approved for public release; distribution is unlimited.</i>			12b. DISTRIBUTION CODE	
13. ABSTRACT (<i>Maximum 200 words</i>) The smaller vertical scales of sound speed variability of several recent deep water Pacific Ocean acoustic experiments are extracted from individual conductivity, temperature, depth (CTD) casts taken along the acoustic paths of these experiments, close to the times of the experiments. The sound speed variability is split into internal wave variability and spice variability, as these two parts obey very different dynamics -- the internal waves move through the water and the spice field moves with the water. Larger scales are mostly responsible for acoustic travel time fluctuations, but smaller scales are mostly responsible for other important phenomena such as intensity and arrival angle fluctuations. A method is presented to determine when the two components are separable. The internal wave properties are consistent with a spectral model such as a generalized Garrett--Munk model, whereas the spice is very intermittent, and the measurements are not extensive enough to confidently make a spice model for acoustic propagation purposes. Both the internal wave results and the spice results are summarized as vertical wavenumber spectra over a selected vertical depth interval, but with the spice, it must be understood that a spectral model would be very different from the data, and that the three-dimensional horizontal--vertical spectrum would be pure conjecture. The spectral level of the (small-scale) spice, averaged over all the profiles, is comparable to that of the internal waves, suggesting that it is not significantly less important to acoustic propagation than are the (small-scale) internal waves.				
14. SUBJECT TERMS internal waves, ocean spice, potential density, potential sound speed, Garrett--Munk spectrum, North Pacific Ocean, Philippine Sea			15. NUMBER OF PAGES 59	
			16. PRICE CODE	
17. SECURITY CLASSIFICATION OF REPORT Unclassified	18. SECURITY CLASSIFICATION OF THIS PAGE Unclassified	19. SECURITY CLASSIFICATION OF ABSTRACT Unclassified	20. LIMITATION OF ABSTRACT SAR	